Cell Reports

Article

Identification and Structure of a Multidonor Class of Head-Directed Influenza-Neutralizing Antibodies Reveal the Mechanism for Its Recurrent Elicitation

Graphical Abstract

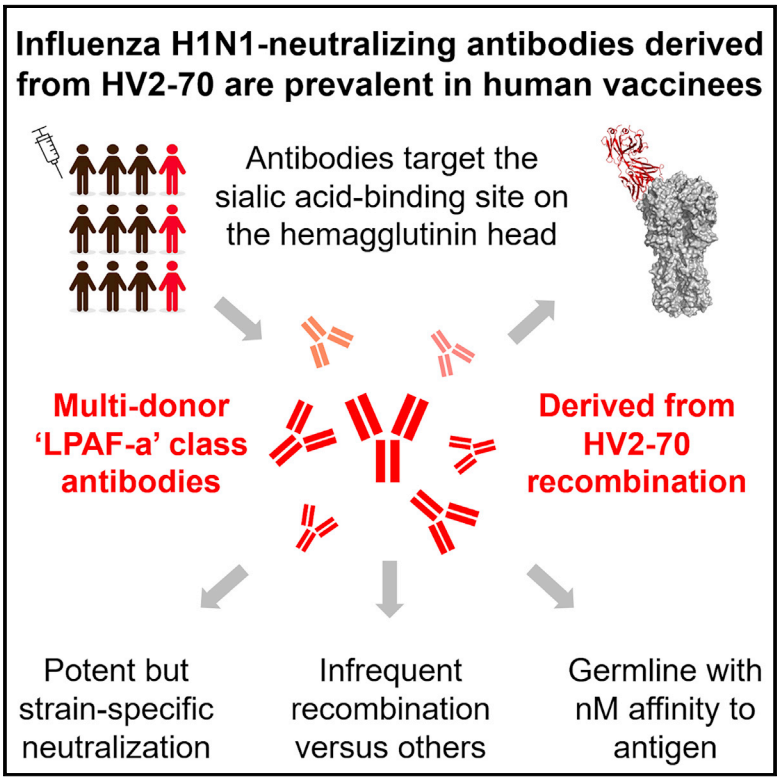

Highlights

- Analysis of HV2-70-derived antibodies reveals basis for a multidonor "LPAF-a" class
- LPAF-a.01 antibody inserts extended CDR H3 into influenza sialic acid-binding site
- Germline-reverted LPAF-a class antibodies have nanomolar affinity for CA09 antigen
- Increased frequency of LPAF-a class antibodies in humans after CA09 vaccination

Authors

Crystal Sao-Fong Cheung, Alexander Fruehwirth, Philipp Carl Georg Paparoditis, ..., Peter D. Kwong, Antonio Lanzavecchia, Tongqing Zhou

Correspondence

pdkwong@nih.gov (P.D.K.), lanzavecchia@irb.usi.ch (A.L.), tzhou@nih.gov (T.Z.)

In Brief

Multidonor influenza-neutralizing antibodies targeting hemagglutinin-head regions may have vaccine utility. Cheung et al. report a HV2-70-derived multidonor class, the "LPAF-a" antibody class, which targets the hemagglutinin head and can be commonly observed in humans after a single vaccination. Recurrent elicitation is attributed to tight binding between hemagglutinin and germline LPAF-a class antibodies.

Cheung et al., 2020, Cell Reports *32*, 108088
September 1, 2020
https://doi.org/10.1016/j.celrep.2020.108088

Cell Reports

CellPress
OPEN ACCESS

Article

Identification and Structure of a Multidonor Class of Head-Directed Influenza-Neutralizing Antibodies Reveal the Mechanism for Its Recurrent Elicitation

Crystal Sao-Fong Cheung,[1,6] Alexander Fruehwirth,[2,6] Philipp Carl Georg Paparoditis,[2] Chen-Hsiang Shen,[1] Mathilde Foglierini,[2] M. Gordon Joyce,[1] Kwanyee Leung,[1] Luca Piccoli,[2] Reda Rawi,[1] Chiara Silacci-Fregni,[2] Yaroslav Tsybovsky,[3] Raffaello Verardi,[1] Lingshu Wang,[1] Shuishu Wang,[1] Eun Sung Yang,[1] Baoshan Zhang,[1] Yi Zhang,[1] Gwo-Yu Chuang,[1] Davide Corti,[2] John R. Mascola,[1] Lawrence Shapiro,[4,5] Peter D. Kwong,[1,5,*] Antonio Lanzavecchia,[2,*] and Tongqing Zhou[1,7,*]

[1]Vaccine Research Center, National Institute of Allergy and Infectious Diseases, National Institutes of Health, Bethesda, MD 20892, USA
[2]Institute for Research in Biomedicine, Università della Svizzera italiana, 6500 Bellinzona, Switzerland
[3]Electron Microscopy Laboratory, Cancer Research Technology Program, Leidos Biomedical Research, Inc., Frederick National Laboratory for Cancer Research, Frederick, MD 21702, USA
[4]Zuckerman Mind Brain Behavior Institute, Columbia University, New York, NY 10027, USA
[5]Department of Biochemistry and Molecular Biophysics, Columbia University, New York, NY 10032, USA
[6]These authors contributed equally
[7]Lead Contact
*Correspondence: pdkwong@nih.gov (P.D.K.), lanzavecchia@irb.usi.ch (A.L.), tzhou@nih.gov (T.Z.)
https://doi.org/10.1016/j.celrep.2020.108088

SUMMARY

Multidonor antibodies are of interest for vaccine design because they can in principle be elicited in the general population by a common set of immunogens. For influenza, multidonor antibodies have been observed against the hemagglutinin (HA) stem, but not the immunodominant HA head. Here, we identify and characterize a multidonor antibody class (LPAF-a class) targeting the HA head. This class exhibits potent viral entry inhibition against H1N1 A/California/04/2009 (CA09) virus. LPAF-a class antibodies derive from the HV2-70 gene and contain a "Tyr-Gly-Asp"-motif, which occludes the HA-sialic acid binding site as revealed by a co-crystal structure with HA. Both germline-reverted and mature LPAF antibodies potently neutralize CA09 virus and have nanomolar affinities for CA09 HA. Moreover, increased frequencies for LPFA-a class antibodies are observed in humans after a single vaccination. Overall, this work highlights the identification of a multidonor class of head-directed influenza-neutralizing antibodies and delineates the mechanism of their recurrent elicitation in humans.

INTRODUCTION

Influenza viruses cause contagious respiratory illness in humans and continue to be a major threat to public health. Recent estimates from the World Health Organization (WHO) indicate that 290,000–650,000 deaths are associated with seasonal influenza epidemics worldwide each year (https://www.cdc.gov/flu/about/burden/preliminary-in-season-estimates.htm). Aside from the yearly outbreaks, influenza viruses have also caused multiple pandemics, resulting in substantial worldwide health and economic burdens (Gilbert, 2018). Despite the availability of vaccines and antiviral drugs, influenza viruses continue to circulate in the human population because of their diversification into novel serotypes and the appearance of pandemic strains. However, even with the yearly development of new seasonal vaccines incorporating the latest circulating strains, the efficacy of these vaccines remains unsatisfactory, ranging from 10% to 60% (https://www.cdc.gov/flu/vaccines-work/past-seasons-estimates.html); as such, there is an urgent need to develop more effective vaccines, both with improved seasonal efficacy and with the ability to neutralize divergent pandemic strains.

An emerging approach to develop effective vaccines against sequence-divergent viruses like influenza and HIV involves antibody lineage-based vaccine design. This approach is predicated on reproducing or "re-eliciting" a selected neutralizing antibody class with priming immunogens that engage the earliest stage of the targeted antibody class followed by subsequent boosting to trigger somatic hypermutation (SHM), thereby leading to maturation of antibodies with high binding affinity and potent neutralizing activity (Kwong and Mascola, 2018). Neutralizing antibodies of the same class develop through similar recombination and maturation pathways and employ the same mode of recognition. Antibodies of the same class can sometimes be found in multiple donors, and a comprehensive understanding of the B cell ontogeny for a particular multidonor antibody may thus provide a framework for the design of immunogens to induce "re-elicitation" of the particular antibody class.

Influenza viruses are classified into four types: A, B, C, and D. Influenza A causes both frequent seasonal epidemics and pandemic outbreaks in humans (Wright et al., 2007). Hemagglutinin (HA) interacts with sialic acid (SA) on the host cell surface, which is a crucial step in virus-cell attachment. Most neutralizing antibodies generated in response to influenza virus infection or vaccination target HA (Altman et al., 2018; Raymond et al., 2018). On the influenza virus, HA is a homotrimer, with each monomer consisting of a globular head and a stem. The HA head is immunodominant over the stem; however, epitopes on the HA head are hypervariable, and therefore neutralizing antibodies elicited against the HA head tend to be strain specific (Dietrich et al., 2017; Sautto et al., 2018). By contrast, antibodies against the conserved stem can be broad, and a number of reproducible classes of stem-directed antibodies have been identified in multiple donors (Ekiert et al., 2009; Joyce et al., 2016). Although several potently neutralizing antibodies targeting the SA receptor binding site (RBS), e.g., CH65 and 1F1 (Tsibane et al., 2012; Whittle et al., 2011), have been identified, these head-directed antibodies have been isolated only from single donors, and no multidonor class of HA head-directed antibodies has been thus far described.

In the current study, we identified a reproducible multidonor class (the LPAF-a class, named after the donor lineage of the most potent initially identified antibody) comprising 28 H1N1 A/California/04/2009 (CA09)-neutralizing antibodies from 3 out of 12 (25%) human vaccinees, each of whom received a single injection of 2010–2011 influenza trivalent inactivated vaccine (TIV). These 28 antibodies derived from the HV2-70 gene paired with four light variable (LV) genes (LV3-21, LV3-9, LV1-36, and LV2-24). The HV2-70 antibodies accounted for approximately 28% of the 98 antibodies isolated from these three donors (Kwong et al., 2017), a substantially higher frequency of HV2-70 antibodies than that observed in the healthy population or in donors from other vaccine trials (Briney et al., 2019; Galson et al., 2016). To understand the recurrent elicitation of this class of antibodies, we produced germline sequence-reverted antibodies and assessed their binding and entry inhibition ability in both microneutralization and pseudovirus assays. We further determined the crystal structure of a LPAF-a lineage antibody in complex with CA09 HA, from which we delineated a sequence signature for the class. We used this signature to calculate the frequency by which antibodies of the LPAF-a class appeared in other vaccination studies, and observed frequencies to increase by greater than 10-fold after CA09 vaccination (Cortina-Ceballos et al., 2015; Galson et al., 2016). Overall, the results reveal how a HA head-directed multidonor class of antibodies can be frequently elicited and, even with a single immunization, can be substantially induced.

RESULTS

Sequences of CA09-Neutralizing Antibodies Isolated from Three TIV Vaccinees Reveal Prevalent HV2-70 Gene Usage

A total of 98 antibodies were isolated from three human vaccinees (FISW, LPAF, and FX) receiving a single immunization of 2010–2011 influenza TIV vaccine. The composition of the 2010–2011 TIV vaccine included A/California/04/2009 (H1N1), A/Perth/16/2009 (H3N2), and B/Brisbane/60/2008. Of the 98 isolated antibodies, 28 (21 from subject FISW, 6 from subject LPAF, and 1 from subject FX) were derived from the same HV2-70 gene (Figure 1A). These HV2-70 antibodies exhibited potent entry inhibition against CA09 and the closely related strain A/Michigan/45/2015 (MI15) in a pseudovirus assay (50% inhibitory concentration [IC_{50}] geometric mean = 7.4 ng/mL for CA09 and 11.7 ng/mL for MI15), but showed only sporadic inhibition against other related H1N1 strains, including A/New Caledonia/20/1999 (NC99), A/New Jersey/1976 (NJ76), and A/South Carolina/01/1918 (SC18), at relatively high concentrations ($p < 0.001$) (Figures 1B and S1; Table S1). To analyze commonalities of these CA09-neutralizing antibodies, we examined the following seven genetic elements: inferred heavy variable (HV), heavy diversity (HD), and heavy joining (HJ) genes; third heavy chain complementarity-determining region (CDR H3) length; inferred LV and light joining (LJ) genes; and third light chain CDR (CDR L3) length (Kwong et al., 2017) (Figure 1C). We found that these 28 HV2-70 influenza antibodies belonged to 17 different lineages, involving the use of four different LV genes, namely, LV3-21, LV3-9, LV1-36, and LV2-24 (Figures 1C, S2, and S3). The CDR H3s (Kabat definition) (Wu and Kabat, 1970) of these HV2-70 antibodies were 12–13 residues in length, whereas the CDR L3s ranged from 9 to 12 residues in length (Figure 1C). Both the HV and LV genes had less than 7% SHM at the nucleotide level. Thus, these 28 CA09-neutralizing antibodies isolated from the three TIV vaccinees were genetically similar.

A Multidonor HV2-70 Antibody Class Targets the SA Receptor Binding Site

To delineate the binding mode of these 28 HV2-70 CA09-neutralizing antibodies, we performed negative stain-electron microscopy (EM) analysis of the purified CA09 HA protein in complex with the antigen-binding fragment (Fab) of a representative member from each of the 17 antibody lineages. Of note, the purified CA09 HA protein appeared to be monomeric instead of trimeric in solution (Figure S4), consistent with a previous study (Yang et al., 2010). EM images showed that the HV2-70 Fabs from each of the 17 lineages bound to the globular head of the HA monomer in a related fashion (Figure 2A). Because each of these antibodies displayed similar genetic components and similar modes of recognition for CA09 HA, we categorized them to be members of the same reproducible or multidonor antibody class, which we named LPAF-a after the most potent identified member lineage.

To further define the epitope of this LPAF-a antibody class, we determined the crystal structure of CA09 HA in complex with the Fab of antibody LPAF-a.01 (named as donor-lineage.clone) at 2.6 Å resolution (Figure 2B; Table S2). The crystallized complex contained one CA09 HA globular head bound to one LPAF-a.01 Fab. Despite the non-trimeric arrangement, the Cα root-mean-square deviation (RMSD) was <0.44 Å versus trimeric HA (PDB: 3UBE) (Xu et al., 2012), and for clarity, we thus depict the LPAF-a.01 complex in the context of a typical HA trimer henceforth (Figure 2C).

LPAF-a.01 bound the CA09 HA globular head through its CDR H1, H2, H3, and CDR L1, L2, and L3 regions (Figure 2C, inset). The heavy chain and light chain contributed 437.6 and

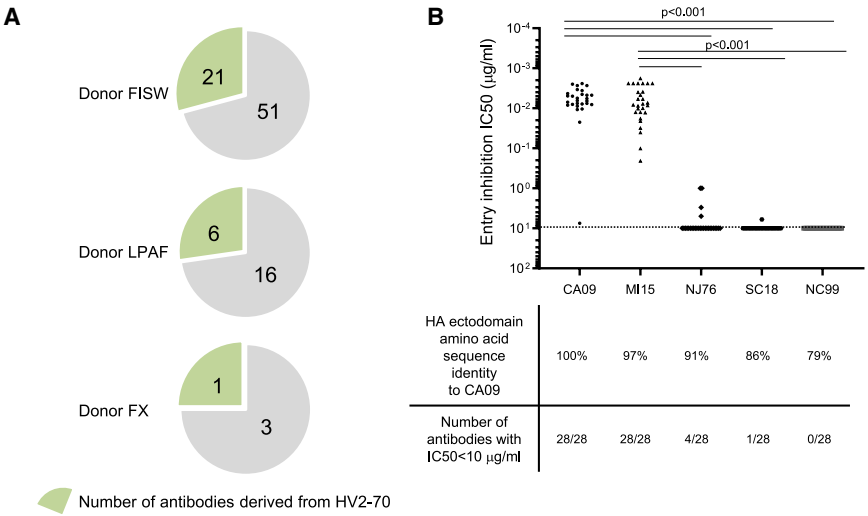

C

Donor	Sequence ID	HV	HD	HJ	HV identities	CDR H3	LV	LJ	LV identities	CDR L3
FISW	FISW-a.01	HV2-70	HD4-17	HJ3	97.3	QLHGDYVRGVFDI	LV3-21	LJ3	95.2	QVWDSSSDHLGV
	FISW-b.01	HV2-70	HD4-17	HJ4	97.0	TLYGDYVSGSFDY	LV3-21	LJ2	96.6	QVWDSSNHYPV
	FISW-c.01	HV2-70	HD4-17	HJ4	96.3	TLYGDYAGGNFDS	LV3-21	LJ2	93.7	QVWDRSSDVV
	FISW-d.01	HV2-70	HD4-17	HJ5	99.0	TYYGDYANWFDP	LV3-21	LJ3	96.5	QVWDSSRDHLWV
	FISW-e.01	HV2-70	HD4-17	HJ4	98.0	SLYGDTLFYFDS	LV3-21	LJ1	96.5	QVWDSSSDHYV
	FISW-e.02	HV2-70	HD4-17	HJ4	97.7	TLYGDTLFYFDS	LV3-21	LJ1	97.2	QVWDSTTDHYV
	FISW-e.03	HV2-70	HD4-17	HJ4	97.0	TLYGDTLYYFDS	LV3-21	LJ1	96.2	QVWDSSSDHYV
	FISW-e.04	HV2-70	HD4-17	HJ4	94.6	SLYGDTLLFFDS	LV3-21	LJ1	95.1	QVCDRSSDQYL
	FISW-f.01	HV2-70	HD4-17	HJ5	97.7	MLYGDFGRYFDP	LV3-21	LJ2	94.8	QVCDTSGYHGV
	FISW-g.01	HV2-70	HD4-17	HJ5	98.0	TLYGDFANYFDP	LV1-36	LJ3	98.6	AAWDDSLNGWV
	FISW-h.01	HV2-70	HD3-10	HJ6	95.6	NNYFDSGYGMDV	LV2-14	LJ2	96.6	TSHTSSSALV
	FISW-i.01	HV2-70	HD4-17	HJ4	99.3	MDYGDFTNYFEY	LV3-9	LJ3	97.2	QVWDSSTAGV
	FISW-j.01	HV2-70	HD4-17	HJ4	97.3	FLYGDFSQYFDY	LV3-9	LJ2	97.5	QVWDSSTVV
	FISW-k.01	HV2-70	HD4-17	HJ5	96.7	KLYGDYSDWFDY	LV3-9	LJ2	97.9	QLSDSSIVV
	FISW-l.01	HV2-70	HD4-17	HJ5	96.6	SYYGDYSNWVDP	LV3-9	LJ1	96.5	QVWDSSTYV
	FISW-l.02	HV2-70	HD4-17	HJ5	95.3	SFYGDFTNWFDP	LV3-9	LJ1	97.5	QVWDSPTYV
	FISW-m.01	HV2-70	HD4-17	HJ5	98.3	HFYGDFGGWFDP	LV3-9	LJ2	95.1	QVRDSNTVV
	FISW-n.01	HV2-70	HD4-17	HJ4	97.3	TLYGDYVSGVSDY	LV3-21	LJ1	96.9	QVWDSSSDHPYV
	FISW-n.02	HV2-70	HD4-17	HJ4	97.0	TLYGDYVGGVSDF	LV3-21	LJ1	95.2	QVWDGSSDHPYV
	FISW-o.01	HV2-70	HD4-17	HJ4	96.7	LRYGDFGRTFDY	LV3-21	LJ2	94.8	QVWESSSDHPVV
	FISW-o.02	HV2-70	HD4-17	HJ4	94.4	LPYGDFGRMFDY	LV3-21	LJ2	96.9	QVWDSSSDHPVV
LPAF	LPAF-a.01	HV2-70	HD4-17	HJ5	95.3	MLYGDLGGRFDP	LV3-9	LJ2	96.4	QVWDSNTVV
	LPAF-a.02	HV2-70	HD4-17	HJ5	96.7	MLYGDFGGYLDP	LV3-9	LJ2	97.1	QVWDSNTVL
	LPAF-a.03	HV2-70	HD4-17	HJ5	95.3	ILYGDFVGYLDP	LV3-9	LJ2	96.8	QVWDTNTVL
	LPAF-a.04	HV2-70	HD4-17	HJ5	94.6	MLYGDLGGRFDP	LV3-9	LJ2	95.4	QVWDSNTVV
	LPAF-a.05	HV2-70	HD4-17	HJ5	94.6	MLYGDFAGYLDP	LV3-9	LJ2	96.0	QVWDSSSVA
	LPAF-a.06	HV2-70	HD4-17	HJ5	92.9	MLYGDIGGWLDP	LV3-9	LJ2	95.4	QVWDSSTVV
FX	FX-a.01	HV2-70	HD4-17	HJ5	99.0	ALYGDYVGYFDP	LV3-21	LJ3	96.9	QVWDSSSHHWV

Figure 1. Analysis of Antibodies from Three Human Vaccinees Showing H1N1 A/California/04/2009 (CA09) Virus Entry Inhibition Reveals Prevalent HV2-70 Gene Usage

(A) Pie chart of the antibody heavy chain gene usage for the influenza antibodies isolated from three TIV vaccinees (FISW, LPAF, and FX). A total of 28 antibodies were derived from the same HV2-70 gene (highlighted in green).

(B) All 28 HV2-70 antibodies showed potent entry inhibition for CA09 and closely related MI15, but poor inhibition for other related H1N1 viruses, including NJ76, SC18, and NC99. The number of virus entry-inhibiting antibodies (IC_{50} cutoff < 10 μg/mL) decreased as the HA ectodomain amino acid sequence identity to CA09 decreased. The horizontal dotted line indicates the highest antibody concentration tested. Experiments were carried out in triplicates. p value, non-parametric Kruskal-Wallis test, corrected for multiple comparison.

(C) Genetic characteristics of the 28 isolated HV2-70 antibodies.

See also Figures S1–S3 and Tables S1 and S6.

393.8 Å^2, respectively, to the overall buried surface area (BSA), as calculated with PISA (Proteins, Interfaces, Structures and Assemblies; https://www.ebi.ac.uk/pdbe/pisa/) (Table S3). The HV2-70 germline-encoded CDR H1 and CDR H2 contributed 122 Å^2 (14.7%) of overall BSA and interacted with the Helix 190 region of HA (Table S4) (Lazniewski et al., 2018; Sriwilaijaroen and Suzuki, 2012). When modeled onto the trimeric HA, CDR H2 residues Trp53 and Asp54 could also be observed to interact with neighboring HA protomer (Table S3). The HD4-17-derived CDR H3 accounted for 315 Å^2 (37.9%) of BSA and interacted mainly with the RBS (Table S4). Interaction of heavy and light chain residues with CA09 HA (Table S3) was annotated on the sequence as shown in Figure 2D.

Comparison of the LPAF-a.01 epitope with the footprint of SA bound to the HA head (PDB: 3UBE) (Xu et al., 2012) indicated they overlapped at the RBS of the HA head domain (Figure 3A). In addition to forming extensive hydrogen bonds with HA residues Ser186, Asp190, Glu227, and Gly228, CDR H3 residue Asp99 at the tip also used its OD2 to mimic the SA atoms O8 and O9 of the host receptor to form a hydrogen bond to the Tyr98 OH of HA (Figure 3B). Mimicry of the SA atom O4 interaction with HA Lys145 atom NZ was also observed for the main-chain carbonyl oxygen of CDR L1 Gly29 and Lys31. Like other RBS-directed antibodies, LPAF-a.01 inserted its CDR H3 into the RBS pocket (Figures 3C and 3D). Comparison of the modes of insertion showed that the CDR H3s reached into the pocket at different depth and with different angles of approach (Figure 3D). Antibodies such as CH65 and H2526 with longer CDR H3s (Schmidt et al., 2015; Whittle et al., 2011) penetrated deeper than LPAF-a.01 with a 12-amino acid-long CDR H3 (Figure 3D). CDR H3 of LPAF-a.01 approached the pocket in a similar way to that of RBS-targeting antibody 8M2 (Xu et al., 2013) to interact with the side of the pocket that contacts the SA O9 region, away from the side that interacted with CDR H3 of CH65 (Whittle et al., 2011) and the SA O4 atom (Figure 3D). We reasoned that LPAF-a.01, like other RBS-targeting antibodies, sterically blocked the interaction of SA with CA09 HA, which in turn resulted in inhibition of viral entry. Structure analysis herein indicated the LPAF-a multidonor antibody class to resemble other CDR H3-dominated antibodies (Bangaru et al., 2019; Hong et al., 2013; Schmidt et al., 2015; Tsibane et al., 2012; Whittle et al., 2011; Winarski et al., 2015; Xu et al., 2013) to insert their CDR H3 loops into the RBS to block SA binding.

LPAF-a Antibody Class Utilizing HV2-70 Has Lower Recombination Frequency Than Influenza Multidonor Classes Derived from HV1-69 or HV6-1

As a consequence of differing recombinations, the 28 LPAF-a antibodies had CDR H3 lengths of 12–13 amino acids (Figure 1C).

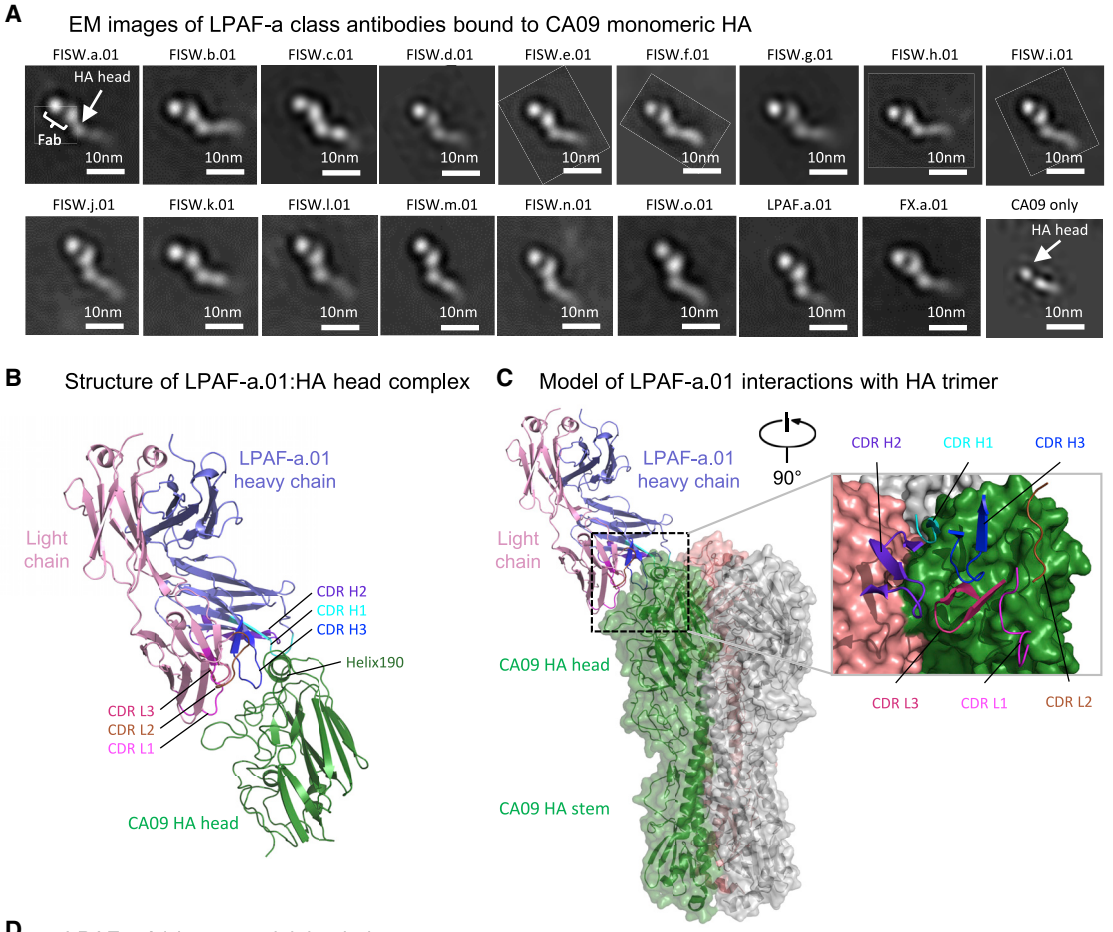

Figure 2. The Reproducible LPAF-a Antibody Class Binds to the Receptor Binding Site of CA09 HA

(A) EM class average images revealed the antibodies binding to the globular head of CA09 HA. One representative antibody from each of the 17 lineages is shown. Scale bar indicates 10 nm in length.

(B) Crystal structure of LPAF-a.01 Fab in complex with CA09 HA. Only the CA09 HA head is present in the crystallized complex. Heavy chain and light chain of LPAF-a.01 were colored slate and light pink with CDR H1, H2, H3, L1, L2, and L3 highlighted in cyan, purple, blue, magenta, brown, and hot pink, respectively.

(C) Model of LPAF-a.01 binding to the CA09 HA trimer (PDB: 3UBE). Only one antibody is shown for clarity. The HA protomer with bound antibody was colored green; the other two protomers of the trimer were colored salmon or gray, respectively. The zoom-in view was rotated 90° to reveal the interactions of CDR loops with the HA surface.

(D) Paratope of antibody LPAF-a.01. Sequences were annotated with Kabat numbering scheme. Heavy and light residues in contact with HA were colored blue or magenta, respectively. ○ denotes main-chain interaction, ☼ denotes side-chain interaction, and ✹ denotes both main- and side-chain interactions. Residues that interacted with neighboring protomer when modeled in the CA09 HA trimer model (PDB: 3UBE) were underlined.

See also Figure S4 and Tables S2 and S3.

Despite this, there was a conserved Tyr-Gly-Asp (YGD) motif in this antibody class at positions 97–99 of the CDR H3, which was fully encoded by the HD4-17 gene (Figure 4A) and provided 66.2% of the CDR H3 BSA (Table S4). Specifically, the Asp99 in CDR H3 interacted with Tyr98 and other residues in the RBS pocket of HA (Figure 3B; Table S3), whereas Tyr97 in CDR H3 formed hydrogen bonds with Thr187 and Glu227 in the RBS (Table S3).

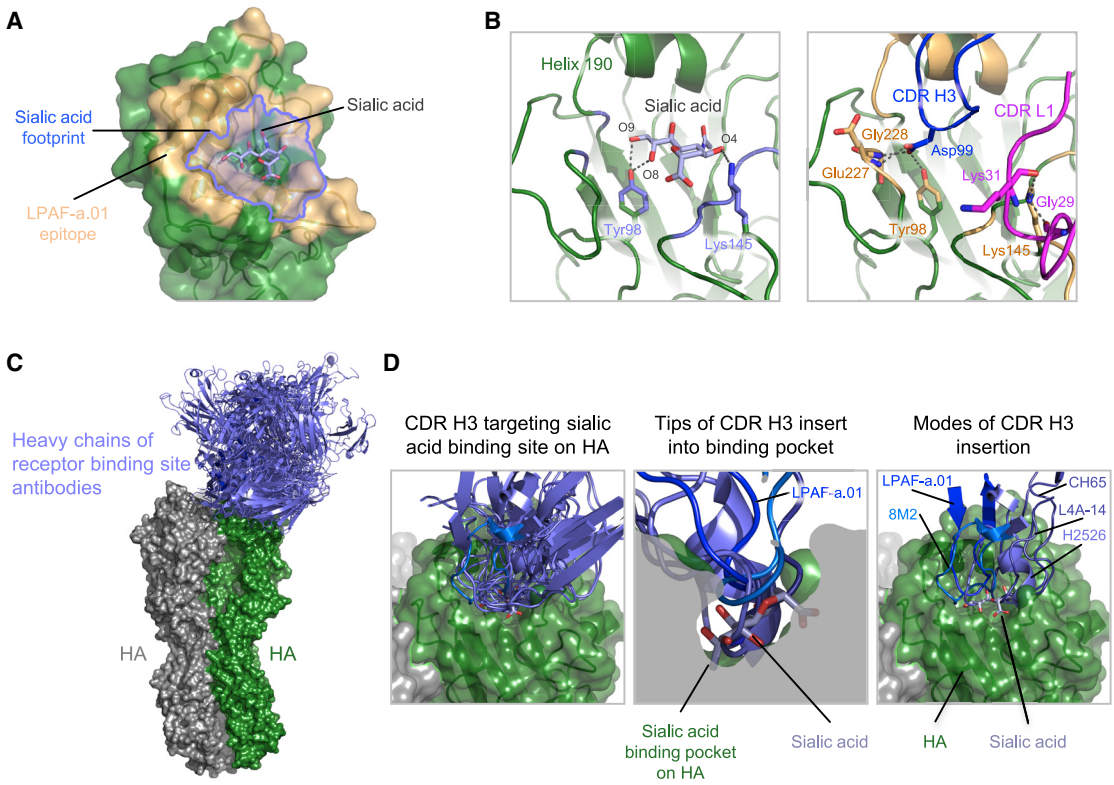

Figure 3. Analysis of Antibody Binding to HA Reveals Similarity of LPAF-a.01 CDR H3 to Those of Other Sialic Acid Binding Site Targeting Antibodies

(A) The LPAF-a.01 epitope (light orange) overlapped with the sialic acid binding site (outlined in slate) on the HA head.

(B) Key HA residues that interacted with both sialic acid (left) and LPAF-a.01 (right). Atom OD2 of Asp99 at the tip of CDR H3 mimicked the sialic acid atoms O8 and O9 to form hydrogen bonds with HA Tyr98. OD1 and OD2 atoms also interacted with main-chain N atoms of HA residues Glu227 and Gly228. HA Lys145, which forms a hydrogen bond with sialic acid atom O4, also interacted with main-chain atom O of CDR L1 residues Gly29 and Lys31. Epitope atoms of LPAF-a.01 on HA were colored light orange.

(C) Sialic acid binding site targeting antibodies approach the HA head in different orientations.

(D) Tips of CDR H3s of LPAF-a.01 (blue) and other antibodies (shades of blue) reach into the sialic acid binding pocket on HA (left). A cutaway surface of the HA SA binding pocket with representative CDR H3s (middle) indicated that LAPF-a.01 did not reach into the pocket as deep as some of the antibodies with long CDR H3s. CDR H3s of antibodies CH65 (PDB: 5UGY) and H2526 (PDB: 4YJZ), which contain 19 and 21 amino acids, can reach as deep as the HA contact plane of the sialic acid ring. Modes on CDR H3 interaction vary by angles of approach and depth of insertion (right).

See also Tables S3 and S4.

Assuming requirements for the LPAF-a class to include both a HV2-70 gene and a HD4-17 gene encoding a YGD motif, we calculated the recombination frequency of the LPAF-a antibody class to be less than 1 in 10^5 (Figure 4B). This is about one-tenth the recombination frequency of the HV6-1 HA stem-targeting antibody class, which contains the very broad 56.a.09 and MEDI8852 antibodies (Joyce et al., 2016; Kallewaard et al., 2016), and is 1,000-fold rarer than the HV1-69 antibody class (Figure 4B), which contains potently neutralizing cross-group antibodies, including F10, CR9114 (Dreyfus et al., 2012), and 27F3 (Avnir et al., 2014; Lang et al., 2017). Despite their high prevalence after CA09 vaccination, the calculated heavy chain-recombination frequency for the LPAF-a class was substantially lower than for other multidonor influenza antibodies.

We also analyzed interactions involving elements encoded by the HV2-70 gene to understand its preferred usage. We found Trp53 in the CDR H2, which is conserved in all 28 isolated LPAF-a class antibodies, to make extensive hydrophobic contacts to Ile219, Cys33, and Tyr97 of CA09 HA. In addition, Asp54, also in the CDR H2, formed a salt bridge with Lys163 of the neighboring HA protomer (Figure 4C, left panel); however, this residue was changed to Asn, Arg, or Glu in some of the 28 isolated antibodies. We noticed that the Trp53-Asp54 motif was not only specific for HV2-70 gene but could also be encoded by the HV2-5 origin gene (Figures 4C and S5).

Ubiquitous Binding of LPAF-a Germline Antibodies to CA09 HA with High Affinity Suggests a Mechanism for Its Recurrent Elicitation

Because both HV and LV genes of the LPAF-a antibodies exhibited low SHM (<7%) (Figure 1C), we examined whether the germline-reverted antibodies would show binding to CA09 HA and entry inhibition against CA09 virus. Biolayer interferometry (BLI) assessment of the LPAF-a germline-reverted and mature

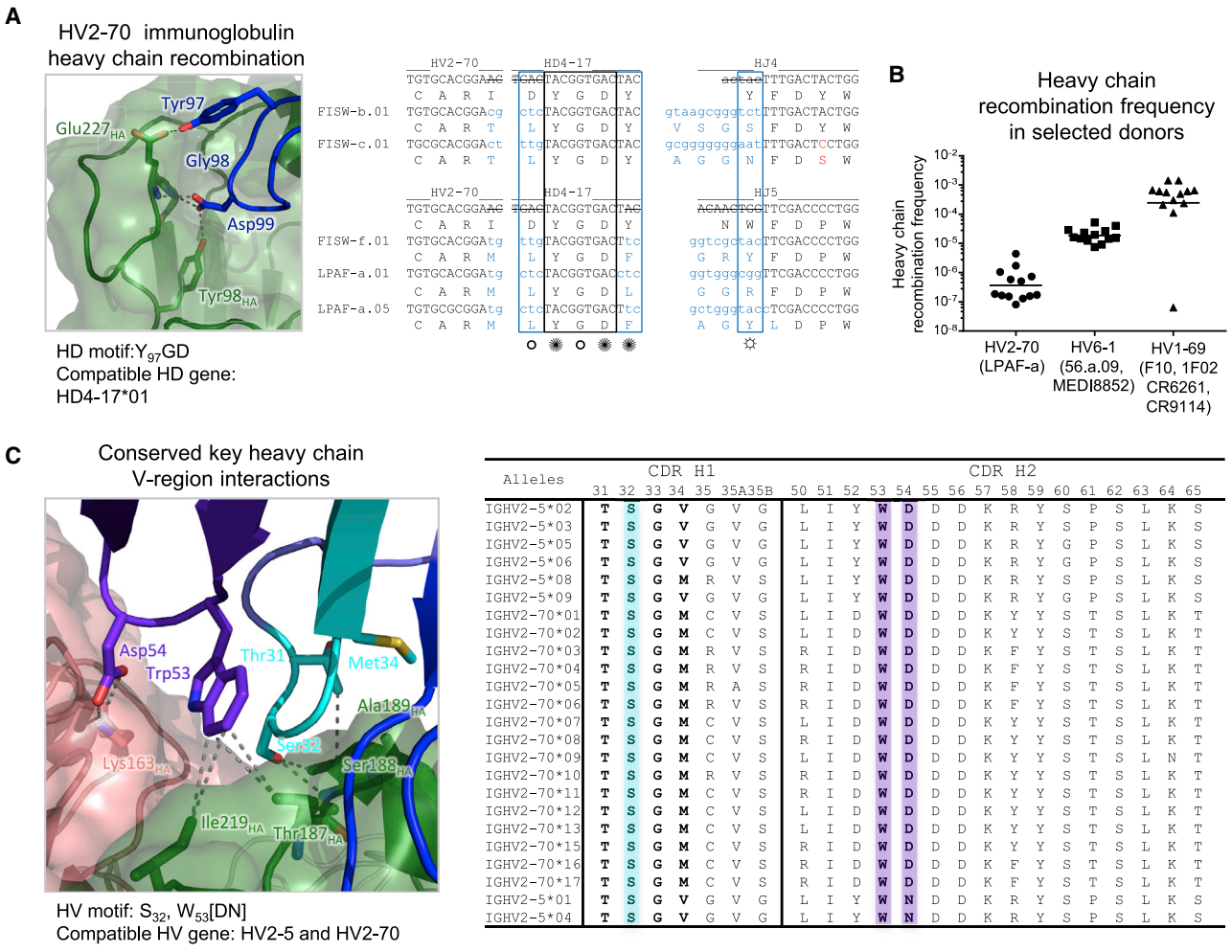

Alleles	CDR H1							CDR H2															
	31	32	33	34	35	35A	35B	50	51	52	53	54	55	56	57	58	59	60	61	62	63	64	65
IGHV2-5*02	T	S	G	V	G	V	G	L	I	Y	W	D	D	D	K	R	Y	S	P	S	L	K	S
IGHV2-5*03	T	S	G	V	G	V	G	L	I	Y	W	D	D	D	K	R	Y	S	P	S	L	K	S
IGHV2-5*05	T	S	G	V	G	V	G	L	I	Y	W	D	D	D	K	R	Y	G	P	S	L	K	S
IGHV2-5*06	T	S	G	V	G	V	G	L	I	Y	W	D	D	D	K	R	Y	G	P	S	L	K	S
IGHV2-5*08	T	S	G	M	R	V	S	L	I	Y	W	D	D	D	K	R	Y	S	P	S	L	K	S
IGHV2-5*09	T	S	G	V	G	V	G	L	I	Y	W	D	D	D	K	R	Y	G	P	S	L	K	S
IGHV2-70*01	T	S	G	M	C	V	S	L	I	D	W	D	D	D	K	Y	Y	S	T	S	L	K	T
IGHV2-70*02	T	S	G	M	C	V	S	L	I	D	W	D	D	D	K	Y	Y	S	T	S	L	K	T
IGHV2-70*03	T	S	G	M	R	V	S	R	I	D	W	D	D	D	K	F	Y	S	T	S	L	K	T
IGHV2-70*04	T	S	G	M	R	V	S	R	I	D	W	D	D	D	K	F	Y	S	T	S	L	K	T
IGHV2-70*05	T	S	G	M	R	A	S	R	I	D	W	D	D	D	K	F	Y	S	T	S	L	K	T
IGHV2-70*06	T	S	G	M	R	V	S	R	I	D	W	D	D	D	K	F	Y	S	T	S	L	K	T
IGHV2-70*07	T	S	G	M	C	V	S	L	I	D	W	D	D	D	K	Y	Y	S	T	S	L	K	T
IGHV2-70*08	T	S	G	M	C	V	S	R	I	D	W	D	D	D	K	Y	Y	S	T	S	L	K	T
IGHV2-70*09	T	S	G	M	C	V	S	L	I	D	W	D	D	D	K	Y	Y	S	T	S	L	N	T
IGHV2-70*10	T	S	G	M	R	V	S	R	I	D	W	D	D	D	K	Y	Y	S	T	S	L	K	T
IGHV2-70*11	T	S	G	M	C	V	S	R	I	D	W	D	D	D	K	Y	Y	S	T	S	L	K	T
IGHV2-70*12	T	S	G	M	C	V	S	L	I	D	W	D	D	D	K	Y	Y	S	T	S	L	K	T
IGHV2-70*13	T	S	G	M	C	V	S	L	I	D	W	D	D	D	K	Y	Y	S	T	S	L	K	T
IGHV2-70*15	T	S	G	M	C	V	S	R	I	D	W	D	D	D	K	Y	Y	S	T	S	L	K	T
IGHV2-70*16	T	S	G	M	C	V	S	R	I	D	W	D	D	D	K	F	Y	S	T	S	L	K	T
IGHV2-70*17	T	S	G	M	C	V	S	R	I	D	W	D	D	D	K	F	Y	S	T	S	L	K	T
IGHV2-5*01	T	S	G	V	G	V	G	L	I	Y	W	N	D	D	K	R	Y	S	P	S	L	K	S
IGHV2-5*04	T	S	G	V	G	V	G	L	I	Y	W	N	D	D	K	R	Y	S	P	S	L	K	S

Figure 4. LPAF-a Antibody Class Heavy Chain Has Lower Recombination Frequency Than Influenza Multidonor Classes Derived from HV1-69 or HV6-1

(A) Sequence signature of the reproducible LPAF-a antibody class includes the usage of HV2-70 gene and the "YGD" motif in CDR H3. Germline HV2-70-, HD4-17-, and HJ4/5-encoded nucleotides and amino acid residues are shown in black, with residues derived from P, N-addition shown in light blue and residues that have undergone SHM in red. Nucleotides removed by exonuclease trimming are indicated with a line through the letters. Conserved HD4-17-encoded residues (YGD) are highlighted by a black box. ☼ denotes antibody side-chain-only contacts, and ✹ denotes both main- and side-chain interactions.

(B) The heavy chain recombination frequencies of HV2-70, HV6-1, and HV1-69 influenza antibody classes calculated by software OLGA. The representative antibodies were listed inside parentheses. See method for the class signatures defined for the calculation of recombination frequency. Bar indicates geometric mean.

(C) Combined structure and sequence analyses reveal conserved HV motif (highlighted in cyan and purplish blue) and compatible heavy chain V germline genes. Bold font indicated compatible paratope residues on heavy chain germline sequences.

See also Figure S4.

antibodies showed that both germline-reverted and mature antibodies bind CA09 HA at nanomolar affinities with an average of 7.1 and 5.2 nM, respectively (Table S6). In addition, we observed both germline-reverted and mature antibodies to exhibit potent entry inhibition of CA09 pseudovirus with IC_{50} of approximately 4.4 and 3.3 ng/mL, respectively (Table S6). Overall, these data suggest that tight HA binding and potent CA09 viral entry inhibition by the LPAF-a class antibodies are present after recombination and without substantial SHM. The high affinity of the initial recombinant and the lack of requirement for SHM provide a mechanism for the recurrent elicitation of this antibody class upon vaccination. Notably, this recurrent elicitation occurs despite relatively low heavy chain recombination frequency.

The LPAF-a.01 Antibody Forms Crucial Interactions with Strain-Specific Residues in the CA09 HA Head

The reproducible LPAF-a antibody class neutralized potently CA09 and MI15, but not other related H1N1 strains (Figure 1B). When we assessed the neutralizing activity of LPAF-a.01 antibody using microneutralization assays with two other CA09 isolates harboring single (K212T) and triple (K123E, A189D, D225G) mutations, we observed the IC_{50} to increase drastically with

these mutations (Figure S6). To understand the strain specificity of the LPAF-a class, we aligned the LPAF-a.01 epitope residues on CA09 HA with other HA proteins from diverse H1N1 influenza viruses and identified several amino acid positions that could explain its specificity (Figure 5A). We produced CA09 HA mutants with LPAF-a.01 epitope residues mutated to the corresponding residues present in NJ76 HA and compared the binding affinities of the wild-type CA09 and CA09 mutants toward the LPAF-a.01 antibody. Two single mutations, K145N and E227A, reduced affinity toward LPAF-a.01 by 17- and 1,500-fold, respectively, whereas other single mutations induced less than 10-fold decrease in affinity of LPAF-a.01 binding (Figure 5B; Table S5). As revealed in the crystal structure, Lys145 formed a salt bridge with CDR L2 residue Asp51, and also formed hydrogen bonds with CDR L1 residues Gly29 and Lys31 of LPAF-a.01. On the other hand, Glu227, which provided ~5% of the epitope surface, formed a hydrogen bond with the conserved CDR H3 residue Tyr97 of the YGD motif (Figure 5C). Hence we showed that LPAF-a.01 antibody interacted with the residues unique to CA09; these residues are also present in closely related MI15, but not in other influenza viral strains tested. This observation may account for the limited neutralization breadth of LPAF-a class.

Vaccination Increases Elicitation Frequency of Antibodies Encoded by Genes Compatible with the Reproducible LPAF-a Class

With the defined signature for the LPAF-a antibody class (Y_{97}GD and 12- to 13-residue CDR H3, HV2-70 gene; Figure 4A), we identified antibodies belonging to the LPAF-a class from two previous influenza vaccination studies from Galson et al. (2016) and Cortina-Ceballos et al. (2015). In the Galson et al. (2016) study, individuals immunized with 2009 monovalent inactivated CA09 virus (MIV) vaccine showed more than 10-fold increase post-vaccination in the frequency of antibodies containing the LPAF-a class sequence signatures (Figure 6A). In the Cortina-Ceballos et al. (2015) study, MIV-immunized subjects showed 38- to 81-fold increase in the LPAF-a class sequences (Figure 6A). Consistent with our current findings, the heavy chain SHM levels of LPAF-a antibodies from both Galson et al. (2016) and Cortina-Ceballos et al. (2015) studies were <5% (Figure 6B). We expressed 29 of these signature-matched HV2-70 LPAF-a class heavy chains paired with either of two light chains, the LPAF-a.01 light chain for 12-residue CDR H3 heavy chains, or the FISW-a.01 light chain for 13-residue CDR H3 heavy chains (Table S7). Twenty-seven of the 29 reconstituted antibodies potently inhibited CA09 viral entry in a pseudovirus assay, with IC_{50} geometric mean of 5.9 ng/mL (Figure 6C). Because the LPAF-a class signature could also be encoded by HV2-5 gene, we also produced six antibodies using the signature-matched HV2-5 LPAF-a class heavy chains (Table S7) and found all of them to exhibit CA09 viral entry inhibition, although with lower potency than the HV2-70 antibodies, with IC_{50} geometric mean of 27.8 ng/mL (Figure 6C). Overall, we observed a significant increase in the frequency of transcripts corresponding to LPAF-a class antibodies after CA09 MIV immunization, suggesting that the frequency of LPAF-a class antibodies could be substantially increased in response to a single vaccination.

DISCUSSION

Multidonor antibodies could in principle form the basis of an effective influenza vaccine. Here, we describe a multidonor antibody class, the LPAF-a class, which was elicited in 3 out of 12 donors (25%) after a single CA09 vaccine immunization. Genetic analysis indicated that the LPAF-a neutralizing antibodies were derived from the HV2-70 gene in all three human donors (Figure 1A). The prevalence of the HV2-70 antibodies identified in the current study was ~28%, which is significantly higher than observed in the normal human population (Briney et al., 2019). X-ray crystallography showed that the D-gene-encoded Y_{97}GD motif present in CDR H3 interacted with the RBS of the HA head to achieve potent CA09 strain-specific neutralization by providing 66% of the CDR H3 paratope BSA (Figures 1, 2, and 3; Table S4). Utilization of common D-gene-encoded motifs has been observed in HA-targeting antibodies derived from different HV genes (Matsuda et al., 2019; Schmidt et al., 2015). Previous studies have shown that the HV3-30-derived antibodies 429 B01 and 39.39, as well as the HV6-1-derived antibodies 56.a.09 and MEDI8852 achieved recognition of conserved epitope on the HA stem using a shared HD3-3-encoded Phe-Gly motif (Matsuda et al., 2019). It is noteworthy that the HD4-17-encoded YGD motif in the LAPF-a class antibodies did not undergo substantial SHM, which potentially enabled germline-reverted antibodies to bind to CA09 HA with high affinity (Table S6). The ability of germline-reverted LPAF-a class antibodies to bind CA09 HA with nanomolar affinities (Table S6) may provide a molecular mechanism for recurrent elicitation of this head-directed antibody class. Indeed, post hoc analysis of two previously published vaccination studies also showed that heavy chain transcripts with a sequence signature matching the LPAF-a class increased in frequency upon a single vaccination, and reconstitution of these transcripts with LPAF-a class light chains yielded potent CA09 pseudovirus neutralization (Figure 6). Given that CA09 is now a reasonably frequent target within current human B memory (at least in adults), we would expect antibodies of this class to be elicited at an even higher frequency in the general population.

Other multidonor antibody classes have been observed to target influenza HA previously. These include multidonor classes that were derived from HV1-69 (Ekiert et al., 2009; Kashyap et al., 2010; Lingwood et al., 2012; Pappas et al., 2014; Sui et al., 2009; Throsby et al., 2008), HV6-1 (Joyce et al., 2016; Kallewaard et al., 2016), and HV1-18 (Andrews et al., 2017; Joyce et al., 2016; Matsuda et al., 2019). These three classes target the conserved HA stem, so the same epitope is present on HAs from diverse influenza viruses. By contrast, the LPAF-a class targets the sequence-diverse head region, with the epitope present only on the CA09 viral strain (Figure 5). Analysis of the crystal structure indicated that essentially all CDRs of LPAF-a.01 were involved in antigen binding, with CDR H3 dominating the interaction by contributing ~38% of the total BSA. Other RBS-targeting antibodies from diverse germline origins have been isolated, and structural studies have revealed different degrees of receptor mimicry by CDR H3 loops of these antibodies (Chen et al., 2017; Ekiert et al., 2012; Fleury et al., 1998; Hong et al., 2013; Huang et al., 2019; Lee et al., 2012; Liu et al., 2017; McCarthy

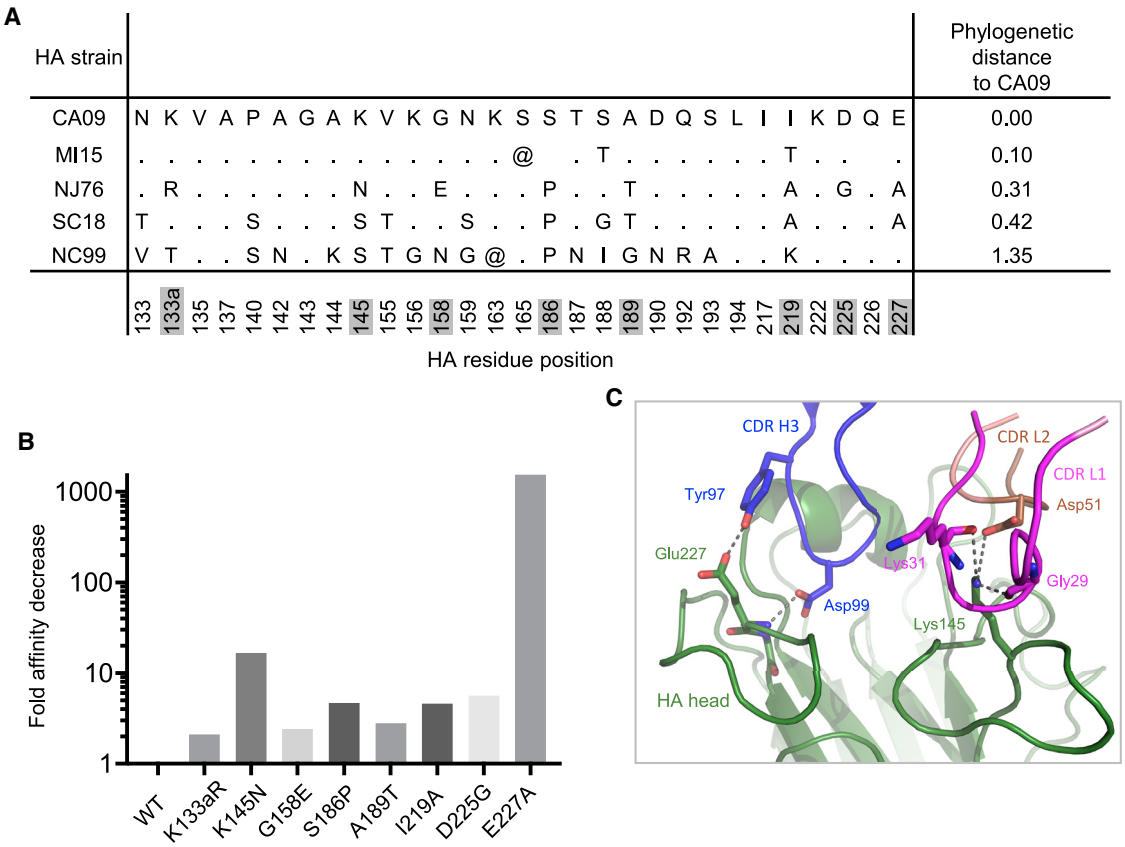

Figure 5. LPAF-a Class Antibodies Showed Strain-Specific Entry Inhibition Because They Interact with HA Residues Unique to CA09

(A) Sequence alignment of LPAF-a.01 epitope residues with diverse HA H1N1 strains. Phylogenetic distance to CA09 is shown in the last column. @ depicts a potential glycosylated asparagine within epitope sequence. Residue numbers are shown at the bottom with specific site mutations highlighted in gray shade.

(B) Effects of strain-specific point mutations in CA09 on binding of the LPAF-a.01 antibody. Eight residues in CA09 HA were mutated to the corresponding amino acids in NJ76, and their fold affinity decrease toward LPAF-a.01 antibody was shown.

(C) Structural basis of critical epitope amino acids in CA09 HA that confer strain specificity.

See also Figure S6 and Table S5.

et al., 2018; Raymond et al., 2016; Schmidt et al., 2013, 2015; Tsibane et al., 2012; Whittle et al., 2011; Xu et al., 2013). Alignment of HA in complex with LPAF-a.01 and other RBS-targeting antibodies showed that all of these antibodies insert CDR H3 loops into the SA binding pocket on HA to occlude the binding of receptor (Figure 3). However, the modes of CDR H3 insertion vary in angle of approach and depth of penetration (Figure 3D). The CDR H3-mediated RBS interactions can be categorized into three types according to the focal areas: (1) to the region of the HA RBS pocket that interacts with SA atom O9, as shown by antibody 8M2 (Xu et al., 2013); (2) to the region of HA RBS pocket that interacts with SA atom O4 on the opposite side, as shown by antibodies CH65 (Whittle et al., 2011) and L4A-14 (Huang et al., 2019); and (3) to the middle of the RBS pocket, as shown by antibodies 1F1 and H2526 (Schmidt et al., 2015; Tsibane et al., 2012). The CDR H3 of LPAF-a.01 targets the RBS pocket to a similar region targeted by antibody 8M2, but it does not reach as deep as other longer CDR H3s (Figure 3D). RBS-targeting antibodies from diverse germline origins have been previously identified, but none of them have been confirmed by sequence and structural studies to belong to any multidonor class. Here, we reported that the LPAF-a class forms a multidonor antibody class that targets the HA head (Table S4).

In summary, the recurrent elicitation of the multidonor class of HV2-70 antibodies may provide insight into the parameters for recurrent elicitation of a multidonor class. Because these antibodies are specific to CA09, they provide a more immunogen-specific readout for elicitation versus the very broad stem-directed antibodies that can be stimulated by most influenza strains and vaccines. Yet, the immunological importance of these antibodies for vaccine development against the head of influenza HA remains to be explored. Overall, it appears that the high affinity of CA09-immunogen to the germline-reverted version of LPAF-a class antibodies may be the critical parameter needed to achieve recurrent elicitation. Indeed, we observed that the LPAF-a class, with its long CDR H3, had substantially lower heavy chain recombination frequencies than other influenza-targeting multidonor antibody classes (Figure 4B). In general, such lower heavy chain recombination frequencies are characteristic of antibodies with focused CDR H3 recognition,

A Prevalence of LPAF-a class and related antibodies in heavy-chain only datasets

Vaccination study	Galson et al.		Cortina-Ceballos et al.	
Vaccine	A/California/04/2009 H1N1, GlaxoSmithKline (non-adjuvanted 15 μg HA, adjuvanted 3.75 μg HA +AS03A oil-in-water emulsion adjuvant)		A/California/04/2009 H1N1, Sanofi Pasteur (non-adjuvanted, 15 μg HA V-like virus)	
Year of vaccination	2010-2011		2011	
Year of sampling	2010-2011		2011	
Samples collected	Pre-pH1N1 (268,768)	7 days post pH1N1 (270,879)	Pre-pH1N1 (259,146)	7 days post-pH1N1 (295,327)
HV2-70, ^{97}YGD, CDR H3: 12-13 a.a.	0.0260%	0.3090%	0.0147%	0.5648%
HV2-5, ^{97}YGD, CDR H3: 12-13 a.a.	0%	0.5061%	0.0012%	0.0979%

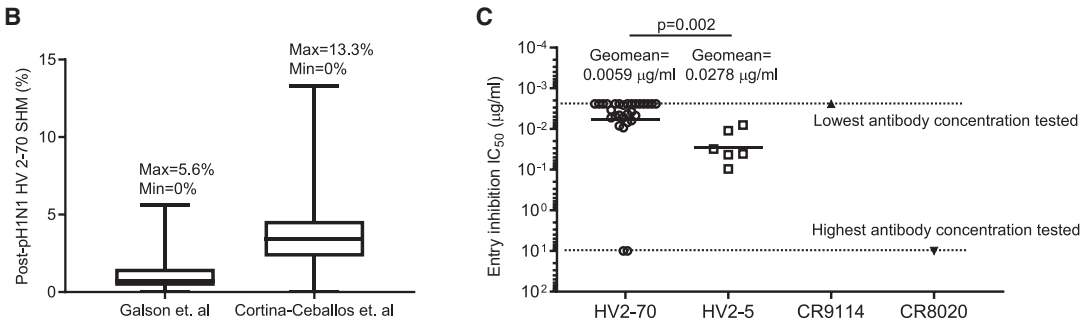

Figure 6. Frequency of Transcripts Compatible with the LPAF-a Antibody Class Increases Upon CA09-HA Vaccination

(A) Bioinformatic search of influenza antibodies in previous vaccination studies based on the defined sequence signature. In both Galson et al. (2016) and Cortina-Ceballos et al. (2015) vaccination studies, the frequency of eliciting these LPAF-a-reproducible antibodies increased 7 days post-H1N1 vaccination.

(B) Box and whisker plot for the LPAF-a class antibodies elicited by vaccination in both Galson et al. (2016) and Cortina-Ceballos et al. (2015) studies showed the very low HV2-70 germline somatic hypermutation rate (SHM). The median is marked in the middle of the box. The maximum (max) and minimum (min) values are labeled.

(C) Over 95% (27 out of 29) of the HV2-70 antibodies and 100% (6 out of 6) of the HV2-5 antibodies containing the defined heavy chain sequence signature showed potent entry inhibition of CA09 pseudovirus. IC_{50} geometric mean of the antibodies was denoted. The cross-group broadly neutralizing antibody CR9114 and group 2-specific antibody CR8020 were used as positive and negative controls, respectively. Experiments were carried out in triplicates. p value, non-parametric Mann-Whitney rank test.

the most common type of antibody recognition. The results presented here provide insight on how such antibodies might be reproducibly elicited, despite their low recombination frequency.

STAR★METHODS

Detailed methods are provided in the online version of this paper and include the following:

- KEY RESOURCES TABLE
- RESOURCE AVAILABILITY
  - Lead Contact
  - Materials Availability
  - Data and Code Availability
- EXPERIMENTAL MODEL AND SUBJECT DETAILS
  - Cell Lines
  - Patient Samples
- METHOD DETAILS
  - Isolation of CA09-reactive human monoclonal antibodies
  - Cloning and production of influenza antibodies
  - Antibody gene assignment, nomenclature and genetic analysis
  - Production of HA-pseudotyped lentiviral vectors and measurement of antibody activity on viral entry inhibition
  - Enzyme-linked immunosorbent assay ELISA
  - H1N1 CA09 virus microneutralization
  - Expression and Purification of CA09 HA
  - Antibody Fab preparation
  - Negative-stain electron microscopy
  - Protein complex crystallization screening
  - X-ray data collection, structure solution, model building and refinement

- Delineation of sequence signatures
- Antibody recombination frequency calculation
- Construction of germline-reverted antibody
- CA09 HA mutagenesis
- Binding affinity measurement by Bio-Layer Interferometry
- Bioinformatics analysis of NGS samples

- QUANTIFICATION AND STATISTICAL ANALYSIS

SUPPLEMENTAL INFORMATION

Supplemental Information can be found online at https://doi.org/10.1016/j.celrep.2020.108088.

ACKNOWLEDGMENTS

We thank J. Stuckey for assistance with figures, and members of the Structural Biology Section and Structural Bioinformatics Core, Vaccine Research Center for discussions and comments on the manuscript. Support for this work was provided by the Intramural Research Program of the Vaccine Research Center, National Institute of Allergy and Infectious Diseases, National Institutes of Health (NIH). This work was also supported in part with federal funds from the Frederick National Laboratory for Cancer Research, NIH, under contract HHSN261200800001 (to Y.T.). The work at the Institute for Research in Biomedicine was supported by the Swiss Vaccine Research Institute, the Swiss National Science Foundation (grant no. 176165), and the European Research Council (grant no. 670955 BROADimmune). Use of sector 22 (Southeast Region Collaborative Access team) at the Advanced Photon Source was supported by the US Department of Energy, Basic Energy Sciences, Office of Science (under contract no. W-31-109-Eng-38).

AUTHOR CONTRIBUTIONS

C.S.-F.C., M.G.J., A.L., L.S., P.D.K., and T.Z. designed experiments. C.S.-F.C., A.F., P.C.G.P., M.F., K.L., L.W., E.S.Y., Y.Z., Y.T., R.V., B.Z., and T.Z. performed the experiments. C.-H.S., R.R., and G.-Y.C. performed computational sequence and structural analyses. D.C., A.F., P.C.G.P., K.L., L.P., C.S.-F., and A.L. contributed critical resources and reagents. C.S.-F.C., S.W., L.S., J.R.M., P.D.K., and T.Z. analyzed the data and wrote the paper, with all authors providing comments.

DECLARATION OF INTERESTS

The authors declare no competing interests.

Received: December 3, 2019
Revised: May 12, 2020
Accepted: August 7, 2020
Published: September 1, 2020

REFERENCES

Adams, P.D., Gopal, K., Grosse-Kunstleve, R.W., Hung, L.W., Ioerger, T.R., McCoy, A.J., Moriarty, N.W., Pai, R.K., Read, R.J., Romo, T.D., et al. (2004). Recent developments in the PHENIX software for automated crystallographic structure determination. J. Synchrotron Radiat. *11*, 53–55.

Adams, P.D., Afonine, P.V., Bunkóczi, G., Chen, V.B., Davis, I.W., Echols, N., Headd, J.J., Hung, L.W., Kapral, G.J., Grosse-Kunstleve, R.W., et al. (2010). PHENIX: a comprehensive Python-based system for macromolecular structure solution. Acta Crystallogr. D Biol. Crystallogr. *66*, 213–221.

Altman, M.O., Angeletti, D., and Yewdell, J.W. (2018). Antibody Immunodominance: The Key to Understanding Influenza Virus Antigenic Drift. Viral Immunol. *31*, 142–149.

Andrews, S.F., Joyce, M.G., Chambers, M.J., Gillespie, R.A., Kanekiyo, M., Leung, K., Yang, E.S., Tsybovsky, Y., Wheatley, A.K., Crank, M.C., et al. (2017). Preferential induction of cross-group influenza A hemagglutinin stem-specific memory B cells after H7N9 immunization in humans. Sci. Immunol. *2*, eaan2676.

Avnir, Y., Tallarico, A.S., Zhu, Q., Bennett, A.S., Connelly, G., Sheehan, J., Sui, J., Fahmy, A., Huang, C.Y., Cadwell, G., et al. (2014). Molecular signatures of hemagglutinin stem-directed heterosubtypic human neutralizing antibodies against influenza A viruses. PLoS Pathog. *10*, e1004103.

Bangaru, S., Lang, S., Schotsaert, M., Vanderven, H.A., Zhu, X., Kose, N., Bombardi, R., Finn, J.A., Kent, S.J., Gilchuk, P., et al. (2019). A Site of Vulnerability on the Influenza Virus Hemagglutinin Head Domain Trimer Interface. Cell *177*, 1136–1152.e18.

Briney, B., Inderbitzin, A., Joyce, C., and Burton, D.R. (2019). Commonality despite exceptional diversity in the baseline human antibody repertoire. Nature *566*, 393–397.

Chen, Z., Bao, L., Chen, C., Zou, T., Xue, Y., Li, F., Lv, Q., Gu, S., Gao, X., Cui, S., et al. (2017). Human Neutralizing Monoclonal Antibody Inhibition of Middle East Respiratory Syndrome Coronavirus Replication in the Common Marmoset. J. Infect. Dis. *215*, 1807–1815.

Cortina-Ceballos, B., Godoy-Lozano, E.E., Téllez-Sosa, J., Ovilla-Muñoz, M., Sámano-Sánchez, H., Aguilar-Salgado, A., Gómez-Barreto, R.E., Valdovinos-Torres, H., López-Martínez, I., Aparicio-Antonio, R., et al. (2015). Longitudinal analysis of the peripheral B cell repertoire reveals unique effects of immunization with a new influenza virus strain. Genome Med. *7*, 124.

Davis, I.W., Murray, L.W., Richardson, J.S., and Richardson, D.C. (2004). MOLPROBITY: structure validation and all-atom contact analysis for nucleic acids and their complexes. Nucleic Acids Res. *32*, W615–W619.

Dietrich, M.H., Harprecht, C., and Stehle, T. (2017). The bulky and the sweet: How neutralizing antibodies and glycan receptors compete for virus binding. Protein Sci. *26*, 2342–2354.

Dreyfus, C., Laursen, N.S., Kwaks, T., Zuijdgeest, D., Khayat, R., Ekiert, D.C., Lee, J.H., Metlagel, Z., Bujny, M.V., Jongeneelen, M., et al. (2012). Highly conserved protective epitopes on influenza B viruses. Science *337*, 1343–1348.

Ekiert, D.C., Bhabha, G., Elsliger, M.A., Friesen, R.H., Jongeneelen, M., Throsby, M., Goudsmit, J., and Wilson, I.A. (2009). Antibody recognition of a highly conserved influenza virus epitope. Science *324*, 246–251.

Ekiert, D.C., Kashyap, A.K., Steel, J., Rubrum, A., Bhabha, G., Khayat, R., Lee, J.H., Dillon, M.A., O'Neil, R.E., Faynboym, A.M., et al. (2012). Cross-neutralization of influenza A viruses mediated by a single antibody loop. Nature *489*, 526–532.

Emsley, P., and Cowtan, K. (2004). Coot: model-building tools for molecular graphics. Acta Crystallogr. D Biol. Crystallogr. *60*, 2126–2132.

Fleury, D., Wharton, S.A., Skehel, J.J., Knossow, M., and Bizebard, T. (1998). Antigen distortion allows influenza virus to escape neutralization. Nat. Struct. Biol. *5*, 119–123.

Fu, L., Niu, B., Zhu, Z., Wu, S., and Li, W. (2012). CD-HIT: accelerated for clustering the next-generation sequencing data. Bioinformatics *28*, 3150–3152.

Galson, J.D., Trück, J., Kelly, D.F., and van der Most, R. (2016). Investigating the effect of AS03 adjuvant on the plasma cell repertoire following pH1N1 influenza vaccination. Sci. Rep. *6*, 37229.

Gilbert, J.A. (2018). Seasonal and pandemic influenza: global fatigue versus global preparedness. Lancet Respir. Med. *6*, 94–95.

Hall, T.A. (1999). BioEdit: a user-friendly biological sequence alignment editor and analysis program for Windows 95/98/NT. Nucleic Acids Symp. Ser. *41*, 95–98.

Hong, M., Lee, P.S., Hoffman, R.M., Zhu, X., Krause, J.C., Laursen, N.S., Yoon, S.I., Song, L., Tussey, L., Crowe, J.E., Jr., et al. (2013). Antibody recognition of the pandemic H1N1 Influenza virus hemagglutinin receptor binding site. J. Virol. *87*, 12471–12480.

Huang, K.A., Rijal, P., Jiang, H., Wang, B., Schimanski, L., Dong, T., Liu, Y.M., Chang, P., Iqbal, M., Wang, M.C., et al. (2019). Structure-function analysis of neutralizing antibodies to H7N9 influenza from naturally infected humans. Nat. Microbiol. *4*, 306–315.

Joyce, M.G., Wheatley, A.K., Thomas, P.V., Chuang, G.Y., Soto, C., Bailer, R.T., Druz, A., Georgiev, I.S., Gillespie, R.A., Kanekiyo, M., et al.; NISC Comparative Sequencing Program (2016). Vaccine-Induced Antibodies that Neutralize Group 1 and Group 2 Influenza A Viruses. Cell *166*, 609–623.

Kallewaard, N.L., Corti, D., Collins, P.J., Neu, U., McAuliffe, J.M., Benjamin, E., Wachter-Rosati, L., Palmer-Hill, F.J., Yuan, A.Q., Walker, P.A., et al. (2016). Structure and Function Analysis of an Antibody Recognizing All Influenza A Subtypes. Cell *166*, 596–608.

Kashyap, A.K., Steel, J., Rubrum, A., Estelles, A., Briante, R., Ilyushina, N.A., Xu, L., Swale, R.E., Faynboym, A.M., Foreman, P.K., et al. (2010). Protection from the 2009 H1N1 pandemic influenza by an antibody from combinatorial survivor-based libraries. PLoS Pathog. *6*, e1000990.

Krissinel, E., and Henrick, K. (2007). Inference of macromolecular assemblies from crystalline state. J. Mol. Biol. *372*, 774–797.

Kwon, Y.D., Chuang, G.Y., Zhang, B., Bailer, R.T., Doria-Rose, N.A., Gindin, T.S., Lin, B., Louder, M.K., McKee, K., O'Dell, S., et al. (2018). Surface-Matrix Screening Identifies Semi-specific Interactions that Improve Potency of a Near Pan-reactive HIV-1-Neutralizing Antibody. Cell Rep. *22*, 1798–1809.

Kwong, P.D., Chuang, G.Y., DeKosky, B.J., Gindin, T., Georgiev, I.S., Lemmin, T., Schramm, C.A., Sheng, Z., Soto, C., Yang, A.S., Mascola, J.R., and Shapiro, L. (2017). Antibodyomics: bioinformatics technologies for understanding B-cell immunity to HIV-1. Immunol Rev *275*, 108–128.

Kwong, P.D., and Mascola, J.R. (2018). HIV-1 Vaccines Based on Antibody Identification, B Cell Ontogeny, and Epitope Structure. Immunity *48*, 855–871.

Lang, S., Xie, J., Zhu, X., Wu, N.C., Lerner, R.A., and Wilson, I.A. (2017). Antibody 27F3 Broadly Targets Influenza A Group 1 and 2 Hemagglutinins through a Further Variation in V_H1-69 Antibody Orientation on the HA Stem. Cell Rep. *20*, 2935–2943.

Lazniewski, M., Dawson, W.K., Szczepinska, T., and Plewczynski, D. (2018). The structural variability of the influenza A hemagglutinin receptor-binding site. Brief. Funct. Genomics *17*, 415–427.

Lee, P.S., Yoshida, R., Ekiert, D.C., Sakai, N., Suzuki, Y., Takada, A., and Wilson, I.A. (2012). Heterosubtypic antibody recognition of the influenza virus hemagglutinin receptor binding site enhanced by avidity. Proc. Natl. Acad. Sci. USA *109*, 17040–17045.

Lefranc, M.P., Giudicelli, V., Duroux, P., Jabado-Michaloud, J., Folch, G., Aouinti, S., Carillon, E., Duvergey, H., Houles, A., Paysan-Lafosse, T., et al. (2015). IMGT®, the international ImMunoGeneTics information system® 25 years on. Nucleic Acids Res. *43*, D413–D422.

Lingwood, D., McTamney, P.M., Yassine, H.M., Whittle, J.R., Guo, X., Boyington, J.C., Wei, C.J., and Nabel, G.J. (2012). Structural and genetic basis for development of broadly neutralizing influenza antibodies. Nature *489*, 566–570.

Liu, Y., Pan, J., Jenni, S., Raymond, D.D., Caradonna, T., Do, K.T., Schmidt, A.G., Harrison, S.C., and Grigorieff, N. (2017). CryoEM Structure of an Influenza Virus Receptor-Binding Site Antibody-Antigen Interface. J. Mol. Biol. *429*, 1829–1839.

Marcatili, P., Rosi, A., and Tramontano, A. (2008). PIGS: automatic prediction of antibody structures. Bioinformatics *24*, 1953–1954.

Marcou, Q., Mora, T., and Walczak, A.M. (2018). High-throughput immune repertoire analysis with IGoR. Nat. Commun. *9*, 561.

Matsuda, K., Huang, J., Zhou, T., Sheng, Z., Kang, B.H., Ishida, E., Griesman, T., Stuccio, S., Bolkhovitinov, L., Wohlbold, T.J., et al. (2019). Prolonged evolution of the memory B cell response induced by a replicating adenovirus-influenza H5 vaccine. Sci. Immunol. *4*, eaau2710.

McCarthy, K.R., Watanabe, A., Kuraoka, M., Do, K.T., McGee, C.E., Sempowski, G.D., Kepler, T.B., Schmidt, A.G., Kelsoe, G., and Harrison, S.C. (2018). Memory B Cells that Cross-React with Group 1 and Group 2 Influenza A Viruses Are Abundant in Adult Human Repertoires. Immunity *48*, 174–184.e9.

Otwinowski, Z., and Minor, W. (1997). Processing of X-ray diffraction data collected in oscillation mode. Methods Enzymol. *276*, 307–326.

Pappas, L., Foglierini, M., Piccoli, L., Kallewaard, N.L., Turrini, F., Silacci, C., Fernandez-Rodriguez, B., Agatic, G., Giacchetto-Sasselli, I., Pellicciotta, G., et al. (2014). Rapid development of broadly influenza neutralizing antibodies through redundant mutations. Nature *516*, 418–422.

Raymond, D.D., Stewart, S.M., Lee, J., Ferdman, J., Bajic, G., Do, K.T., Ernandes, M.J., Suphaphiphat, P., Settembre, E.C., Dormitzer, P.R., et al. (2016). Influenza immunization elicits antibodies specific for an egg-adapted vaccine strain. Nat. Med. *22*, 1465–1469.

Raymond, D.D., Bajic, G., Ferdman, J., Suphaphiphat, P., Settembre, E.C., Moody, M.A., Schmidt, A.G., and Harrison, S.C. (2018). Conserved epitope on influenza-virus hemagglutinin head defined by a vaccine-induced antibody. Proc. Natl. Acad. Sci. USA *115*, 168–173.

Sautto, G.A., Kirchenbaum, G.A., and Ross, T.M. (2018). Towards a universal influenza vaccine: different approaches for one goal. Virol. J. *15*, 17.

Scheres, S.H. (2012). RELION: implementation of a Bayesian approach to cryo-EM structure determination. J. Struct. Biol. *180*, 519–530.

Schmidt, A.G., Xu, H., Khan, A.R., O'Donnell, T., Khurana, S., King, L.R., Manischewitz, J., Golding, H., Suphaphiphat, P., Carfi, A., et al. (2013). Preconfiguration of the antigen-binding site during affinity maturation of a broadly neutralizing influenza virus antibody. Proc. Natl. Acad. Sci. USA *110*, 264–269.

Schmidt, A.G., Therkelsen, M.D., Stewart, S., Kepler, T.B., Liao, H.X., Moody, M.A., Haynes, B.F., and Harrison, S.C. (2015). Viral receptor-binding site antibodies with diverse germline origins. Cell *161*, 1026–1034.

Sethna, Z., Elhanati, Y., Callan, C.G., Walczak, A.M., and Mora, T. (2019). OLGA: fast computation of generation probabilities of B- and T-cell receptor amino acid sequences and motifs. Bioinformatics *35*, 2974–2981.

Sriwilaijaroen, N., and Suzuki, Y. (2012). Molecular basis of the structure and function of H1 hemagglutinin of influenza virus. Proc. Jpn. Acad., Ser. B, Phys. Biol. Sci. *88*, 226–249.

Sui, J., Hwang, W.C., Perez, S., Wei, G., Aird, D., Chen, L.M., Santelli, E., Stec, B., Cadwell, G., Ali, M., et al. (2009). Structural and functional bases for broad-spectrum neutralization of avian and human influenza A viruses. Nat. Struct. Mol. Biol. *16*, 265–273.

Throsby, M., van den Brink, E., Jongeneelen, M., Poon, L.L., Alard, P., Cornelissen, L., Bakker, A., Cox, F., van Deventer, E., Guan, Y., et al. (2008). Heterosubtypic neutralizing monoclonal antibodies cross-protective against H5N1 and H1N1 recovered from human IgM+ memory B cells. PLoS ONE *3*, e3942.

Tiller, T., Meffre, E., Yurasov, S., Tsuiji, M., Nussenzweig, M.C., and Wardemann, H. (2008). Efficient generation of monoclonal antibodies from single human B cells by single cell RT-PCR and expression vector cloning. J. Immunol. Methods *329*, 112–124.

Traggiai, E., Becker, S., Subbarao, K., Kolesnikova, L., Uematsu, Y., Gismondo, M.R., Murphy, B.R., Rappuoli, R., and Lanzavecchia, A. (2004). An efficient method to make human monoclonal antibodies from memory B cells: potent neutralization of SARS coronavirus. Nat. Med. *10*, 871–875.

Tsibane, T., Ekiert, D.C., Krause, J.C., Martinez, O., Crowe, J.E., Jr., Wilson, I.A., and Basler, C.F. (2012). Influenza human monoclonal antibody 1F1 interacts with three major antigenic sites and residues mediating human receptor specificity in H1N1 viruses. PLoS Pathog. *8*, e1003067.

Whittle, J.R., Zhang, R., Khurana, S., King, L.R., Manischewitz, J., Golding, H., Dormitzer, P.R., Haynes, B.F., Walter, E.B., Moody, M.A., et al. (2011). Broadly neutralizing human antibody that recognizes the receptor-binding pocket of influenza virus hemagglutinin. Proc. Natl. Acad. Sci. USA *108*, 14216–14221.

Whittle, J.R., Wheatley, A.K., Wu, L., Lingwood, D., Kanekiyo, M., Ma, S.S., Narpala, S.R., Yassine, H.M., Frank, G.M., Yewdell, J.W., et al. (2014). Flow cytometry reveals that H5N1 vaccination elicits cross-reactive stem-directed antibodies from multiple Ig heavy-chain lineages. J. Virol. *88*, 4047–4057.

Winarski, K.L., Thornburg, N.J., Yu, Y., Sapparapu, G., Crowe, J.E., Jr., and Spiller, B.W. (2015). Vaccine-elicited antibody that neutralizes H5N1 influenza and variants binds the receptor site and polymorphic sites. Proc. Natl. Acad. Sci. USA *112*, 9346–9351.

Wright, P.F., Neumann, G., and Kawaoka, Y. (2007). Orthomyxoviruses. In Fields Virology, D.M. Knipe and P.M. Howley, eds. (Lippincott Williams & Wilkins), pp. 1691–1740.

Wu, T.T., and Kabat, E.A. (1970). An analysis of the sequences of the variable regions of Bence Jones proteins and myeloma light chains and their implications for antibody complementarity. J. Exp. Med. *132*, 211–250.

Xu, R., McBride, R., Nycholat, C.M., Paulson, J.C., and Wilson, I.A. (2012). Structural characterization of the hemagglutinin receptor specificity from the 2009 H1N1 influenza pandemic. J. Virol. *86*, 982–990.

Xu, R., Krause, J.C., McBride, R., Paulson, J.C., Crowe, J.E., Jr., and Wilson, I.A. (2013). A recurring motif for antibody recognition of the receptor-binding site of influenza hemagglutinin. Nat. Struct. Mol. Biol. *20*, 363–370.

Yang, Z.Y., Huang, Y., Ganesh, L., Leung, K., Kong, W.P., Schwartz, O., Subbarao, K., and Nabel, G.J. (2004). pH-dependent entry of severe acute respiratory syndrome coronavirus is mediated by the spike glycoprotein and enhanced by dendritic cell transfer through DC-SIGN. J. Virol. *78*, 5642–5650.

Yang, H., Carney, P., and Stevens, J. (2010). Structure and Receptor binding properties of a pandemic H1N1 virus hemagglutinin. PLoS Curr. *2*, RRN1152.

Ye, J., Ma, N., Madden, T.L., and Ostell, J.M. (2013). IgBLAST: an immunoglobulin variable domain sequence analysis tool. Nucleic Acids Res. *41*, W34–W40.

STAR★METHODS

KEY RESOURCES TABLE

REAGENT or RESOURCE	SOURCE	IDENTIFIER
Antibodies		
28 HV2-70 antibodies from three human donors (FISW, LPAF, FX)	This study	N/A
29 HV2-70 heavy chains	Galson et al., 2016 Cortina-Ceballos et al., 2015	N/A
3 HV2-5 heavy chains	Galson et al., 2016 Cortina-Ceballos et al., 2015	N/A
Virus Strains		
H1N1 A/California/04/2009	NIH/VRC	N/A
H1N1 A/Michigan/45/2015	NIH/VRC	N/A
H1N1 A/New Caledonia/20/1999	NIH/VRC	N/A
H1N1 A/New Jersey/1976	NIH/VRC	N/A
H1N1 A/South Carolina/01/1918	NIH/VRC	N/A
Biological Samples		
PBMC of donors FISW, LPAF, FX	This paper	N/A
Chemicals, Peptides, Recombinant Proteins and Biosensors		
CD22-FITC	BD PharMingen	Cat# 555424; RRID:AB_395818
Anti IgG-APC	Jackson Immunoresearch	Cat# 109-136-088; RRID:AB_2337691
Turbo293 transfection reagent	SPEED BioSystem	Cat# PXX1002
AbBooster medium	ABI scientific	Cat# PB2668
Cell culture lysis buffer	Promega	Cat# E1531
Luciferase assay reagent	Promega	Cat# E1500
Recombinant H1 CA09 protein	Protein Sciences	Cat# NR-44074
Bovine serum albumin	Sigma	Cat# A2058
Anti-total IgG-alkaline peroxidase antibody	Southern Biotechnologies	Cat# OB2041-04
p-nitrophenyl phosphate	Sigma	Cat# 487663
2′-(4-Methylumbelliferyl)-alpha-D-N-aceylneuramainic acid sodium salt hydrate	Sigma	Cat# 8639
Fugene6	Promega	Cat# E2691
COmplete His-Tag Resin	Roche	Cat# 05893801001
Recombinant Protein A Sepharose	GE Healthcare	Cat# 17-1279-03
IgG elution buffer	Thermo Scientific	Cat# 21009
HEPES	Life Technologies	Cat# 15630-080
Sodium chloride	Quality Biological, Inc	Cat# 351-036-101
Protease inhibitor cocktail tablets	Roche	Cat#37378900
Thrombin	Millipore	Cat# 2964423
Endoproteinase LysC	Roche	Cat# 11058533103
Endoglycosidase H	New England Biolabs	Cat# P0702L
Ammonium sulfate	Rigaku Reagents	Cat# 1008359
PEG 8000	Rigaku Reagents	Cat# 1008063
Glycerol	Invitrogen	Cat# 15514-011
Ni-NTA Capture Biosensors	fortéBIO	Cat# 18-5103

(*Continued on next page*)

Continued

REAGENT or RESOURCE	SOURCE	IDENTIFIER
Critical Commercial Assays		
DNA gene synthesis and cloning	GenScript Biotech Corporation	N/A
Site-directed mutagenesis	GeneImmune Biotechnology LLC	N/A
Deposited Data		
Crystal structure of CA09 HA in complex with LPAF-a.01 Fab	This paper	PDB: 6URM
DNA sequences of HV2-70 antibodies	This paper	Heavy chain: GenBank: MT755747, MT755748, MT755749, MT755750, MT755751, MT755752, MT755753, MT755754, MT755755, MT755756, MT755757, MT755758, MT755759, MT755760, MT755761, MT755762, MT755763, MT755764, MT755765, MT755766, MT755767, MT755768, MT755769, MT755770, MT755771, MT755772, MT755773, MT755774
DNA sequences of HV2-70 antibodies	This paper	Light chain: GenBank: MT755775, MT755776, MT755777, MT755778, MT755779, MT755780, MT755781, MT755782
Experimental Models: Cell Lines		
Dog: Madin-Darby Canine Kidney (MDCK) Epithelial Cells	ATCC	Cat# CCL-34; RRID:CVCL_0422
Human HEK293T/17 cells	ATCC	Cat# CRL-11268
Human: FreeStyle 293-F cells	Thermo Fisher	Cat# R79007
Human: Expi293F cells	Thermo Fisher	Cat# A14527; RRID: CVCL_D615
Human: HEK293S GnTI- cells	ATCC	Cat# CRL-3022; RRID: VCL_A785
Recombinant DNA		
pCMV-ΔR8.2	NIH/VRC	N/A
pHR'CMV-Luc	NIH/VRC	N/A
pCMV Sport/h TMPRSS2	NIH/VRC	N/A
human IgG1 expression vector	NIH/VRC	N/A
Lambda light chain expression vector	NIH/VRC	N/A
Kappa light chain expression vector	NIH/VRC	N/A
pVRC8400 vector	NIH/VRC	N/A
Software and Algorithms		
GraphPad Prism 8.0 Software	GraphPad Prism, Inc.	N/A
ForteBio Data Analysis 9.0 software	ForteBio, Inc.	N/A
HKL2000	HKL Research, Inc.	https://www.hkl-xray.com/
Phenix	Adams et al., 2004	https://sbgrid.org/software/
Coot	Emsley and Cowtan, 2004	https://sbgrid.org/software/
Pymol	Schrödinger	https://pymol.org/2/
Relion	Scheres, 2012	https://www3.mrc-lmb.cam.ac.uk/relion/index.php/Main_Page
PRISM 7	GraphPad Software	https://www.graphpad.com/scientific-software/prism/
Dendroscope 3	Daniel H. Huson	http://dendroscope.org
BioEdit v7.2.5	Hall, 1999	https://bioedit.software.informer.com/download/
IMGT	Lefranc et al., 2015	http://www.imgt.org
PDBePISA	Krissinel and Henrick, 2007	https://www.ebi.ac.uk/pdbe/pisa/
OLGA	Sethna et al., 2019	https://github.com/statbiophys/OLGA

RESOURCE AVAILABILITY

Lead Contact

Further information and requests for resources and reagents should be directed to and will be fulfilled by the Lead Contact, Tongqing Zhou (tzhou@nih.gov).

Materials Availability

This study did not generate new unique reagents.

Data and Code Availability

The 28 HV2-70 antibody sequences isolated from the three human vaccinees are listed in Figure S3, and the accession numbers for the nucleotide sequences reported in this paper are GenBank: MT755747, MT755748, MT755749, MT755750, MT755751, MT755752, MT755753, MT755754, MT755755, MT755756, MT755757, MT755758, MT755759, MT755760, MT755761, MT755762, MT755763, MT755764, MT755765, MT755766, MT755767, MT755768, MT755769, MT755770, MT755771, MT755772, MT755773, MT755774, MT755775, MT755776, MT755777, MT755778, MT755779, MT755780, MT755781, MT755782. The HV2-70 and HV2-5 protein sequences are shown in Table S7. Coordinates and structure factors for the protein complex structure reported in this paper have been deposited with the Protein Data Bank and the accession number is PDB: 6URM.

EXPERIMENTAL MODEL AND SUBJECT DETAILS

Cell Lines

Madin-Darby canine kidney (MDCK) cells were purchased from ATCC (cat# CCL-34) and cultured in MEM medium. HEK293T cells were obtained from ATCC (cat# CRL-11268) and cultured in DMEM. FreeStyle 293-F (cat# R79007) and Expi293F cells (cat# A14528; RRID: CVCL_D615) were purchased from ThermoFisher Scientific Inc. FreeStyle 293-F cells were maintained in FreeStyle 293 Expression Medium, while Expi293F cells were maintained in Expi Expression Medium. HEK293S GnTI- cells (cat# CRL-3022 from ATCC) were adapted for suspension culture in FreeStyle 293 Expression Medium. The above cell lines were used directly from the commercial sources and cultured according to manufacturer suggestions.

Patient Samples

Peripheral blood mononuclear cells (PBMC) were obtained from healthy donors before and two weeks after vaccination with the seasonal influenza vaccine. All donors gave written informed consent for research use of blood samples, following approval by the Cantonal Ethical Committee of Cantone Ticino. The genders of the three human donors in the current study are: FISW (female), LPAF (male) and FX (male).

METHOD DETAILS

Isolation of CA09-reactive human monoclonal antibodies

Fresh or cryopreserved PBMC were surface stained with anti CD22-FITC (BD PharMingen) as well as anti IgG-APC (Jackson Immunoresearch) and enriched via anti-FITC microbeads (Miltenyi Biotec). The cell-sorted $CD22^{+}IgG^{+}$ fraction of memory B cells was immortalized with Epstein-Barr virus (EBV), CpG 2006 and cultured at limiting dilutions on irradiated allogeneic PBMC as previously described (Traggiai et al., 2004). Supernatants of immortalized and expanded memory B cells were screened after fourteen days in ELISA assays for specific binding to CA09 HA. Positive cultures were expanded for further studies and characterizations. Immunoglobulin heavy chain or light chain sequences from positive cultures were retrieved via reverse transcriptase PCR (RT-PCR) and sent for sequencing (Microsynth AG, Switzerland).

Cloning and production of influenza antibodies

Immunoglobulin heavy chain or light chain sequences were constructed by gene synthesis and then cloned into human IgG1, lambda, or kappa expression plasmids as previously described (Tiller et al., 2008; Whittle et al., 2014). Heavy and light chain expression plasmid DNA was transfected into Expi293F cells (Thermo Fisher) in 1:1 (v/v) ratio using Turbo293 transfection reagent (Speed BioSystems) (Kwon et al., 2018). Monoclonal antibodies from the culture supernatants were purified using recombinant Protein-A Sepharose (GE Healthcare) as per the manufacturer's instructions.

Antibody gene assignment, nomenclature and genetic analysis

Antibody sequences were annotated using IgBlast (Ye et al., 2013). Antibodies sharing both heavy and light chain V and J gene assignments and junction region were grouped into one lineage. Monoclonal antibodies were named as donor-lineage.clone, i.e., LPAF-a.01 indicates a clonal member ''01'' in lineage ''a'' from the donor LPAF. We noticed that *IGHD2-21* was first D germline gene assigned to FISW-o.01; however, the second and third possible D germline gene were *IGHD4-17*, which differed by alignments. Thus, we used *IGHD4-17* as assigned D germline gene for FISW-o.01.

Production of HA-pseudotyped lentiviral vectors and measurement of antibody activity on viral entry inhibition

Influenza HA pseudotyped lentiviral vectors expressing a luciferase reporter gene were produced as described (Yang et al., 2004). Briefly, HEK293T cells seeded in a 15cm dish were transfected with the following plasmids: 17.5 μg of pCMV-ΔR8.2, 17.5 μg of pHR'CMV-Luc, 0.3 μg pCMV Sport/h TMPRSS2, 1 μg of HA from H1 A/South Carolina/01/1918, H1 A/New Jersey/1976, H1 A/New Caledonia/20/1999, or H1 A/California/04/2009; and 0.125 μg of the corresponding neuraminidase (NA). Cells were transfected overnight by Fugene6 (Promega) and then replaced with fresh medium. Supernatants containing the pseudoviruses were harvested 48 hours post-transfection, filtered, aliquoted and frozen at −80°C before use.

The viral entry inhibition assays were carried out as follow. Serial dilutions of monoclonal antibodies were mixed with titrated pseudoviruses, and then added to 96-well white/black isoplates (PerkinElmer) in triplicate. After incubation for 45 minutes at 37°C, 293T cells (10,000 cells per well) were added to the plates. Following two hours of incubation, 100 μL of fresh medium was added. Cells were lysed 72 hours later in 20 μL of cell culture lysis buffer (Promega). 50 μL of luciferase assay reagent (Promega) was subsequently added to each well. Luciferase activity was measured according to relative light unit (RLU) by MicroBeta luminescence counter (PerkinElmer). IC_{50} were generated using Prism 8.0 (GraphPad).

Enzyme-linked immunosorbent assay ELISA

Half-area ELISA plates (Corning) were coated with 1 μg/ml recombinant H1 protein (H1 A/California/04/2009) (Protein Sciences) in PBS overnight at 4°C and blocked subsequently for one hour with 1% bovine serum albumin (Sigma) in PBS at room temperature. Quadruplicates of serial dilutions of antibodies were incubated for one hour at room temperature and stained, after washing, with an anti-total IgG-alkaline peroxidase antibody (Southern Biotechnologies). Development of the plates was done after an additional washing step by adding 40 μl p-nitrophenyl phosphate substrate (Sigma) and reading them after 30 minutes at room temperature without light at 405nm. Binding affinities were determined using Prism by extrapolating the concentration at which the antibody reaches 50% of the maximum signal (EC_{50}) via four-parameter nonlinear regression with a variable slope.

H1N1 CA09 virus microneutralization

In-vitro viral neutralization assays were performed by preincubating a serial dilution of antibody supernatant with 2000 $TCID_{50}$/ml of A/California/04/2009 (H1N1) virus for one hour at 37°C and then used to infect cultured Madin-Darby canine kidney (MDCK) cells, in MEM infection medium (MEM +Glutamax +Eagle Salts, Kanamycin 1%, TPCK-treated Trypsin 2 μg/ml) (GIBCO). Readout was performed after three days of infection-medium culture by assaying the released Neuraminidase activity conversion of fluorescent substrate solution (2′-(4-Methylumbelliferyl)-alpha-D-N-aceylneuramainic acid sodium salt hydrate (Sigma)) in reaction buffer. Substrate was added to transferred supernatants in black Opaque 96-well plates (Perkin Elmer), and after one hour of incubation at 37°C determined at EX 355nm/EM 460nm with an Envision Fluorometer (PerkinElmer). The neutralization titer (50% inhibitory concentration (IC_{50})) is expressed as the antibody concentration that reduced the fluorescence signal by 50% compared with cell virus only control wells. The IC_{50} values were calculated by interpolation of neutralization curves fitted with a four-parameter nonlinear regression with a variable slope. All antibodies were tested in quadruplicates.

Expression and Purification of CA09 HA

CA09 HA construct C-terminally fused to a thrombin cleavage sequence, T4 fibritin trimerization motif, and a hexahistidine affinity tag were synthesized (Genscript) and cloned into a pVRC8400 expression plasmid as previously described (Whittle et al., 2014). Expi293 cells were diluted to 1.2×10^6 cells/ml and transfected with 500 μg/liter of HA expression plasmids using Turbo293 transfection reagent. At day five, the media was clarified by centrifugation at 2,000 × g and filtered, concentrated, and loaded on Complete His-Tag Resin (Roche) by gravity flow. The resin was washed with three column volumes of PBS with 50 mM imidazole (Roche) and the target protein was subsequently eluted in three column volumes of PBS with 300 mM imidazole. The eluted protein was concentrated and loaded on a Superdex 200 16/60 size exclusion column (GE Healthcare). Fractions corresponding to monomeric CA09 HA were collected, pooled and concentrated. Removal of the His-tag from the CA09 HA protein was performed by digestion with thrombin enzyme (1:1000 w/w) (Millipore) at RT overnight. The untagged CA09 protein was further purified on a Superdex 200 16/60 column and saved for crystallization study.

Antibody Fab preparation

The purified human IgG proteins were cleaved by LysC enzyme (1:4000 w/w) (Roche) at 37°C overnight for Fab preparation. The enzymatic digestion reaction was stopped by adding in protease inhibitor (Roche). The cleavage mixture was passed through a protein A column to separate the Fc fragments from the Fab. The Fab collected in the flow-through was further purified by a Superdex 200 16/60 column in either PBS for binding and neutralization assays, or in a buffer containing 5 mM HEPES pH 7.5 and 150 mM NaCl for crystallization study.

Negative-stain electron microscopy

HA constructs were mixed with Fab fragments at a ratio of two Fab fragments to one HA monomer, followed by an incubation for 1 hour at 4°C. Samples were then diluted with a buffer containing 10 mM HEPES, pH 7.0, and 150 mM NaCl to a concentration of approximately 0.01 mg/ml and applied to a freshly glow-discharged carbon-coated grid. The grid was washed with the same buffer,

and the adsorbed proteins were stained with 0.7% uranyl formate. Micrographs were collected at a nominal magnification of 57,000 on a ThermoFisher Talos F200C electron microscope operating at 200 kV and equipped with a Ceta CCD camera. The pixel size was 0.25 nm/px. Particles were picked automatically using in-house written software (Y.T., unpublished data), as well as manually, and extracted into 144x144-pixel boxes. Reference-free 2D classification was performed using Relion (Scheres, 2012).

Protein complex crystallization screening

Purified CA09 HA protein was mixed with the LPAF-a.01 Fab in a 1:1.2 molar ratio, and then digested with 1:5000 (w/w) EndoH (New England Biolabs) at pH 6.1 at RT for two hours. The protein complex was purified by a Superdex 200 16/60 column in a buffer containing 5 mM HEPES pH 7.5 (Life Technologies) and 150 mM NaCl (Quality Biological, Inc.), and concentrated to a final protein complex concentration of approximately 12 mg/ml. The resulting protein complex was subsequently screened for crystallization hits with Hampton Research, Wizard, and QIAGEN crystal screening kits using a Mosquito crystallization robot. Crystals initially observed from the wells were manually reproduced. CA09 HA-LPAF-a.01 Fab protein complex crystal grew in 0.2 M NH_4SO_4 and 23.57% (w/v) PEG 8000. Optimized crystals were cryoprotected in 30% glycerol and flash-frozen in liquid nitrogen for data collection.

X-ray data collection, structure solution, model building and refinement

X-ray data were collected at a wavelength of 1.00 Å at the SER-CAT beamline ID-22 (Advanced Photon Source, Argonne National Laboratory). Diffraction data were processed with the HKL2000 suite (Otwinowski and Minor, 1997). Structure solution was obtained by molecular replacement with Phaser using search models consisting of the LAPF-a.01 variable region generated with PIGSpro (Marcatili et al., 2008), the constant region of VRC-PG20 Fab (PDB ID: 4LSU) for the lambda light chain and the HA head region (PDB ID: 5K9O). Refinement was carried out with Phenix (Adams et al., 2010). Model building was carried out with Coot (Emsley and Cowtan, 2004). The Ramachandran plot was determined by MOLPROBITY (Davis et al., 2004). Data collection and refinement statistics are shown in Table S2.

Delineation of sequence signatures

We performed a structure-based process to identify sequence signatures for the HV2-70 class CA09-neutralizing antibodies. We observed fifteen distinct memory B cell lineages, from subjects FSIW, LPAF, and FX, to share heavy chain sequences derived from a recombination of HV2-70 with HD4-17, and HJ4 or HJ5, to yield highly similar amino acid sequences in the CDR H3. These fifteen lineages have a CDR H3 length of 12-13 amino acids (Kabat number) and a conserved ^{97}YGD motif. The HV2-70 heavy chain paired with different light chain V genes, including LV1-36, LV3-9, LV3-21, and LV2-14. Structural analysis of LPAF-a.01, a prototypic antibody of this class, revealed that heavy chain binding involved the HD4-17-encoded CDR H3 with Gly98 and Asp99 contributing ~176 Å^2 of BSA (Figure 4A). In addition, Trp53 and Asp54 from CDR H2, which are well conserved among all 28 antibodies for binding to CA09 HA, were included as part of the signature. With that, HV2-5 and HV2-70D genes could also be the potential the germline genes. However, we excluded HV2-70D germline gene because HV2-70D*14 is reported from the study in Africa, and HV2-70D*04 nucleotide sequence is identical to *IGHV2-70*04*.

Antibody recombination frequency calculation

The heavy chain NGS data of thirteen healthy donors were downloaded from https://github.com/crowelab/PyIR and https://github.com/briney/grp_paper. Non-productive sequences were sieved to serve as the dataset for IGOR to inference the model (Marcou et al., 2018). The models were used by OLGA to compute probability of having specific CDR H3 recombination (Sethna et al., 2019). The recombination frequency of LPAF-a class antibody was calculated by masking HV2-70, ^{99}YGD and 12 −13 aa on CDR H3. For 56.a.09 antibody, germline HV6-1, ^{100}FG and 14-16 aa were applied for CDR H3 signature. For antibody class using HV1-69 gene, such as F10, CR9114, and 70-1F02, the *IGHV1-69* alleles with 54F being marked as required V germline gene, 98Y and 12-17 aa CDR H3 were applied. We noticed an outlier in the recombination frequency of *IGHV1-69* alleles. We examined the germline gene assignment of NGS reads and found that both *IGHV1-69* alleles in outlier do not have Phe54.

Construction of germline-reverted antibody

The Kabat schematic was used to define the framework of antibody. We reverted somatically mutated residues that are inside V and J gene regions to germline amino acids but kept the mature CDR 3 sequences in the germline-reverted antibody.

CA09 HA mutagenesis

CA09 HA construct C-terminally fused to a thrombin cleavage sequence, T4 fibritin trimerization motif, and a hexahistidine affinity tag were used as a template for mutagenesis. Eight different single amino acids on the CA09 HA epitope were mutated to the corresponding residues from the most phylogenetically similar NJ76 HA. The resulted CA09 mutant variants were expressed and purified as previously described, and subsequently used for the Octet binding assay.

Binding affinity measurement by Bio-Layer Interferometry

The hexahistidine affinity tagged CA09 HA protein (30 μg/ml) diluted in PBS containing 1% bovine serum albumin was captured on Ni-NTA sensor tips to a level of approximately 1.0 – 1.2nm. The duration of protein capture was 300 s. The sensor tips were then washed

with PBS with 1% bovine serum albumin for 120 s. After washing, the sensor tips were dipped into the Fab with eight different concentrations (200 nM, 100 nM, 50 nM, 25 nM, 12.5 nM, 6.25 nM, 3.125 nM, 0 nM) for an association length of 300 s. After Fab binding, the sensors were placed back into PBS with 1% bovine serum albumin for a dissociation length of 300 s. Antibody binding experiment was performed on a ForteBio OcteRed 96 machine. Subsequent data analysis was performed using the ForteBio Data Analysis 9.0 software.

Bioinformatics analysis of NGS samples

Two next-generation sequencing (NGS) samples from flu vaccine trials were obtained using accession number PRJNA336096 (Galson et al., 2016) and PRJNA301150 (Cortina-Ceballos et al., 2015). Germline genes were assigned to all reads using IgBlast (Ye et al., 2013). For samples used with the 454-pyrosequencing platform, we discarded all reads shorter than 330 nucleotides, having stop codon, and non-productive sequences. For the Illumina MiSeq paired heavy and light chain dataset, we filtered out the reads shorter than 330 nucleotides, having stop codon, and non-productive sequences, then singleton reads in the remaining sequences were removed.

The filtered NGS reads were separated into pre- and post-CA09 influenza-vaccinated sets. Reads were further analyzed for the heavy chain germline genes HV2-70 and HV2-5, CDR H3 length of 12 – 13 amino acids (Kabat notion), and a sequence signature "YGD" in the CDR H3 junction. We used CD-HIT to cluster filtered reads based on their CDR H3 nucleotide sequence (Fu et al., 2012). The CD-HIT parameters, identity and sequence coverage threshold were set to 90% and 97%, respectively. We selected centroid sequence of each cluster paired with light chain of LPAF-a.01 for neutralization assay. In cases of using framework 1 primers in the PCR, we used amino acids from the germline V gene to recover the n-terminal framework region.

QUANTIFICATION AND STATISTICAL ANALYSIS

To calculate statistical significance, non-parametric Kruskal-Wallis test and non-parametric Mann-Whitney rank test were used. Software GraphPad Prism 8.0 was used for statistical analysis.